Monthly Notices of the ROYAL ASTRONOMICAL SOCIETY
MNRAS **546,** 1–16 (2026) https://doi.org/10.1093/mnras/staf1921

Observational constraints of diffusive dark-fluid cosmology

Shambel Sahlu [1,2]★ Upala Mukhopadhyay,[3] Remudin R. Mekuria [4] and Amare Abebe [1,2]

[1] *Centre for Space Research, North-West University, Potchefstroom 2520, South Africa*
[2] *National Institute for Theoretical and Computational Sciences (NITheCS), South Africa*
[3] *Department of Physics and Materials Science, University of Luxembourg, L-1511 Luxembourg City, Luxembourg*
[4] *Faculty of Engineering and Computer Science, Ala-Too International University, Bishkek, Kyrgyzstan*

Accepted 2025 November 2. Received 2025 October 28; in original form 2025 July 30

ABSTRACT

In this manuscript, we investigate late-time cosmology and the evolution of cosmic structures using an interacting dark fluid model in which dark matter (DM) and dark energy (DE) interact through a diffusive mechanism. To provide a comprehensive understanding, we derive the background evolution and perturbation equations within this model and obtain cosmological parameters through MCMC simulations. We use recent measurements for statistical analysis and constrain the parameters H_0 in km s^{-1} Mpc^{-1}, $\Omega_{\rm m}$, $r_{\rm d}$, M, σ_8, S_8, and the interaction term $Q_{\rm dm}$. From the constrained values of $Q_{\rm dm}$, we show that the diffusive model is a promising alternative DE model, capable of driving late-time cosmic acceleration due to energy exchange from DM to DE. State-finder diagnostics indicate that the model behaves like a Chaplygin gas when energy transfers from DM to DE during the Universe's expansion. We also investigate the growth of density contrast, finding $\delta_{\rm m}(z) \gg \delta_{\rm de}(z)$, which highlights the dominant role of DM in structure formation. Redshift space distortion and growth rate analysis show that minor deviations from Lambda cold dark matter at low redshifts, with larger differences at higher redshifts, indicate the impact of energy diffusion on early structure growth. Finally, we perform a detailed statistical analysis, including $\mathcal{L}(\hat{\Theta}|\text{data})$, χ^2, AIC, and BIC, which strongly supports the proposed diffusive dark-fluid model.

Key words: cosmological parameters – dark energy – cosmology: observations – cosmology: theory.

1 INTRODUCTION

The mysterious matter and energy in the Universe, referred to as dark matter (DM) and dark energy (DE), respectively, account for a whopping 95 per cent of the universe's total content. The nature of these dark components of the Universe is not properly understood, but several candidates in the literature, including unified dark-fluid models, have been proposed to describe them and their effect on astrophysics and cosmology. On the DM side, the most commonly studied candidates include Weakly Interacting Massive Particles (WIMPS) (S. Colafrancesco, S. Profumo & P. Ullio 2006; L. Bergström 2009; R. R. Mekuria 2017, 2019; R. R. Mekuria et al. 2017) or some astrophysical modification of gravity such as Modified Newtonian Dynamics (MOND)(M. Milgrom 1983) among many others, whereas on the DE side, the cosmological constant Λ (S. M. Carroll 2001) is perhaps the simplest addition to the standard cosmological model needed to explain most of the observed data. However, there are some serious issues associated with the cosmological constant, such as the eponymous *cosmological constant problem* (S. Weinberg 1989), the coincidence problem (H. E. Velten et al. 2014), the Hubble tension (E. Di Valentino et al. 2021c), the S_8 tension (E. Di Valentino et al. 2021a), the *James Webb Space Telescope* high redshift massive galaxy tensions (I. Labbe et al. 2023), etc., which makes the choice less attractive. That is why there are currently a plethora of other alternatives to explain current cosmological observations, such as modifications to the gravitational theory itself (see e.g. K. Bamba et al. 2012; E. N. Saridakis et al. 2021 and references therein), an evolving Λ (P. Peebles & B. Ratra 1988; P. J. Peebles 1999), deviations from the standard homogeneous (see A. Krasinski 1997; K. Bolejko et al. 2011 and references therein) and isotropic Universe (such as the various Bianchi cosmological models) assumption, or some form of a combination of these, among others.

Another aspect that has gained much traction recently is the interaction of DM and DE (W. Zimdahl 2005; Y. L. Bolotin et al. 2015; U. Mukhopadhyay et al. 2020, 2021; A. Chakraborty et al. 2025). Such an approach is interesting because it has the potential to explain the cosmological and coincidence problems, the Hubble tension, and the S_8 discrepancy (R. C. Nunes & S. Vagnozzi 2021). Some theoretical conditions that such interactions have to satisfy for physical viability have been studied in M. A. Westhuizen & A. Abebe (2024). Diffusive dark-fluid cosmology proposes that DM and DE are different phases of a unified dark fluid, with a diffusion process that allows energy or mass to flow between them (A. Arbey 2006). In recent decades, interacting dark-fluid models have garnered significant attention in cosmology, with extensive studies exploring their various aspects. In particular, investigations of dark-fluid interactions have aimed to address the cosmic coincidence problem (B. Wang et al. 2016). Furthermore, cosmological evolution is broadly discussed in Y. L. Bolotin et al. (2015) and G. S. Sharov

★ E-mail: sahlushambel@gmail.com

et al. (2017) in the interaction between DE and DM. Detailed thermodynamic stability analysis of diffusive dark fluid has been studied in recent work (S. Maity et al. 2019). The work in B. Wang et al. (2007) and Y. Zhai et al. (2023) reported the effect of the interaction between DM and DE on the formation of large-scale structures. This effect is clearly shown at the lowest pole l of the Cosmic Microwave Background (CMB) spectrum.

The diffusive dark fluid is also proposed to alleviate the cosmological tensions as presented in S. Calogero & H. Velten (2013), W. Yang & L. Xu (2014), and R. C. Nunes et al. (2016). Earlier in the Universe, this fluid behaves like DM, helping to form structures, while later it acts like DE, driving cosmic acceleration (T. Zhang & X. Li 2007). The model modifies standard cosmological equations and offers a unified approach to explaining DM and energy. While it simplifies the overall picture, it requires careful tuning of parameters to match observations like the CMB and galaxy surveys. Understanding the rate and underlying causes of this acceleration is crucial for forecasting the ultimate fate of the Universe, whether it will expand indefinitely or face a 'big rip'. Furthermore, the discrepancy in Hubble constant measurements suggests the need for new physics or highlights potential errors in current observational methods. This accelerated expansion also challenges Einstein's theory of general relativity (GR), encouraging cosmologists to propose beyond GR theory for more accurate explanations without the need for a cosmological constant or DE. For instance, the CG model (J. Fabris, S. Goncalves & P. De Souza 2002; M. C. Bento et al. 2002a, b, 2004; M. d. C. Bento et al. 2003; S. Sahlu et al. 2019b, 2023) suggests that an exotic matter with negative pressure could serve as both DM and DE, while the phantom model (E. Elizalde et al. 2004; C. Csaki et al. 2006) proposes a more negative pressure form of DE, leading to accelerating acceleration and super-exponential expansion. Additionally, various modified gravity theories, such as $f(R)$ gravity, based on the Ricci scalar R (A. Abebe et al. 2012a, 2013; S. Bahamonde et al. 2017), $f(Q)$ gravity, where Q is a non-metric (R. Solanki et al. 2022; S. Sahlu et al. 2025a; S. Sahlu, Á. Cruz-Dombriz & A. Abebe 2025b), $f(T)$ gravity, involving the torsion scalar T (R. Myrzakulov 2011; V. F. Cardone et al. 2012; S. Sahlu et al. 2020) just mentioned few, have been proposed to explain the accelerating expansion of the Universe.

In the current work, we investigate the background evolution and cosmological perturbations within the framework of diffusive dark fluid interaction. Our analysis utilizes various recent cosmological data sets, including: (a) BAO distance and correlation measurements from the DR2 data release of the Dark Energy Spectroscopic Instrument Survey (*DESI DR2 BAO*) (M. Abdul-Karim et al. 2025; U. Andrade, E. Paillas et al. 2025); (b) cosmic chronometers (*CC*) data (M. Moresco et al. 2020; J.-Z. Qi et al. 2023), which measure the Hubble parameter $H(z)$ based on the relative ages of massive, early-time, passively evolving galaxies; (c) Type Ia supernovae (SNIa) data sets, specifically: (i) the PantheonPlus+ sample (D. Brout et al. 2022), consisting of 1701 light curves of 1550 distinct SNIa across a redshift range of $z \in [0.001, 2.26]$ (*PPS*); (ii) the *DESY5* data set (R. Chiba & T. J. Moriya 2024), a photometrically classified SNIa with redshifts between 0.1 and 1.13, supplemented by 194 low-redshift SNe Ia spanning $0.025 < z < 0.1$; and (iii) the latest Union3 compilation, which includes 2087 cosmologically useful SNIa from 24 data sets (D. Rubin et al. 2025). We also consider, the redshift-space distortion data (RSD) and the growth rate f, from the VIMOS Public Extragalactic Redshift Survey (VIPERS) and SDSS collaborations. To achieve this, we focus on the theoretical framework of late-time and perturbations, as investigated by considering the diffusive dark fluid model that unifies DM and DE through a diffusive interaction, leading to a coupled evolution that drives cosmic evolution. For better analysis, we use the combined data sets: *DESI DR2 BAO* + *CC* + *DESY5* + *RSD* + f, *DESI DR2 BAO* + *CC* + *Union3* + *RSD* + f and *PPS* + *CC* + *DESY5* + *RSD* + f for constraining the cosmological parameters: H_0, Ω_m, r_d, M, σ_8, S_8 and the interaction term Q_{dm} through the MCMC method. Then we highlighted the values of the Hubble parameter H_0 and matter clustering S_8 to emphasize the possibilities of the diffusive model in mitigating cosmological tensions. *However, addressing the cosmological tensions is beyond the current manuscript.* After constraining the parameters through the MCMC method, different background cosmological quantities namely: the acceleration parameter $q(z)$, the effective equation of state (EoS) parameter $w_{eff}(z)$, the Hubble parameter $H(z)$, and the distance modulus $\mu(z)$ have been illustrated in the diffusive dark-fluid model. The state finder diagnostic plots, q versus r and s versus r are also highlighted for the case of positive and negative Q_{dm} (energy flow from DM to DE and vis versa), offering insights into cosmic expansion and the diffusive dark-fluid model compared to the standard Lambda cold dark matter (ΛCDM) model. The positive Q_{dm} case corresponds to a quintessence-like phase, resulting in a slower expansion, while the negative Q_{dm} case resembles the CG model, leading to faster expansion in the late-time Universe than ΛCDM model. We are also devoted to investigating the $Om(z)$ diagnostic, which plays a significant role in cosmology by offering a model-independent approach to differentiate between various cosmological models, particularly about the nature of DE and the expansion history of the Universe. Its primary function is to help distinguish the standard ΛCDM model from the alternative DE, such as the diffusive model. In the case of ΛCDM where DE is modelled as a cosmological constant, $Om(z)$ is expected to remain nearly constant across different redshifts. On the whole, the diffusive dark-fluid model indicates a Universe in which DE may not be a straightforward cosmological constant but rather a dynamically changing phenomenon across time. This might lead to an improved understanding of cosmic acceleration and challenge the simplicity of the traditional ΛCDM model.

We also employ cosmic perturbation theory as a tool to understand how the large-scale structures we observe today have evolved and expanded as a result of gravitational instabilities in the early Universe. In the standard metric perturbation theory pioneered by Lifshitz (E. M. Lifshitz 1946) and later refined by Bardeen (J. M. Bardeen 1980) and Kodama and Sasaki (H. Kodama & M. Sasaki 1984), one usually starts by perturbing away from a homogeneous and isotropic background metric. The 1+3-covariant and gauge-invariant perturbation formalism (S. W. Hawking 1966; D. Olson 1976; G. F. Ellis & M. Bruni 1989a; M. Bruni et al. 1992; P. K. Dunsby et al. 1992; P. Dunsby, M. Bruni & G. Ellis 1992), on the other hand, starts by defining covariant and gauge-invariant gradient variables that define fluctuations in a given cosmological quantity (such as the energy density and the volume expansion; G. F. Ellis & M. Bruni 1989a; S. Carloni et al. 2008; A. Abebe et al. 2012b) without specifying the background metric from the start.[1] This paper also focuses on analysing linear cosmological perturbations to explore how the diffusive dark fluid model impacts the development of large-scale structures in the Universe. We have implemented the 1+3 covariant formalism introduced by S. W. Hawking (1966), D. Olson (1976), G. F. Ellis & M. Bruni (1989a,

[1] See (A. A. Gidelew 2009) and the references therein for more details on this and the pros and cons of the two approaches of cosmological perturbation theory.

b), G. Ellis, M. Bruni & J. Hwang (1990), M. Bruni et al. (1992), P. K. Dunsby et al. (1992), P. Dunsby et al. (1992), which distinguishes between time and space through an observer's four-velocity u^a and the projection tensor h_{ab}. This approach streamlines the examination of space–time and matter dynamics. Important quantities in this framework include the expansion scalar Θ, shear σ_{ab}, and vorticity ω_{ab}, which characterize cosmic expansion, shape distortions, and rotational effects. This formalism also allows for the decomposition of the energy-momentum tensor (EMT), facilitating the analysis of perturbations, structure formation, the CMB, and the expansion of the Universe, particularly within modified gravity models. The evolution equation for the density contrast $\delta_m(z)$ is examined using the 1+3 formalism across various gravity theories including GR (P. Dunsby et al. 1992), $f(R)$ gravity (A. Abebe et al. 2012a, 2013), $f(T)$ gravity (S. Sahlu et al. 2020; H. Sami et al. 2021), $f(Q)$ gravity (S. Sahlu et al. 2025a, b), the CG model (S. Sahlu et al. 2023), the $f(R, L_{\rm m})$ gravity (S. Sahlu et al. 2024) and scalar-tensor theories (J. Ntahompagaze et al. 2018, 2020) to study the growth of cosmic structures. In the current work, we also implement the same manner for the diffusive model to study the scalar perturbations, which leads to an enhanced understanding of the structure growth of the Universe. In addition, a detailed statistical analysis of $\mathcal{L}(\hat{\Theta}|\text{data})$, χ^2, χ^2_ν, AIC, ΔAIC, BIC, and ΔBIC has been carried out to validate the diffusive dark fluid model's performance.

We organize the rest of the manuscript as follows: In Section 2, we talk about the theory of the covariant thermodynamic description and come up with the field equations for the background Universe, focusing on the diffusive dark-fluid system. In this section, the full set of evolution equations is derived for the linear cosmological perturbation using the 1+3 covariant formalism. The evolution equations of the density contrast $\delta(z)$ and the redshift space distortion $f\sigma_8(z)$ are presented to allow us to study structure formation. The constraining of cosmological parameters from MCMC simulations is done in Section 3 after the full sets of equations for the background and perturbation have been put in order. In this section, the numerical results of the work are broadly explained. This section also includes a statistical analysis of the work. Finally, in Section 4, the conclusions are presented.

2 THEORETICAL FRAMEWORK

Fundamentally, the standard ΛCDM cosmology arises as a solution to the Einstein field equations (EFEs), derived from the action:

$$S = \frac{c^4}{16\pi G}\int \mathrm{d}^4x\sqrt{-g}\,[R + 2\,(L_{\rm m} - \Lambda)]\,, \tag{1}$$

where R is the Ricci scalar, $L_{\rm m}$ is the matter Lagrangian density, and Λ is the cosmological constant. Then the corresponding EFEs are expressed as

$$G_{\mu\nu} + \Lambda g_{\mu\nu} = 8\pi G T_{\mu\nu}\,, \tag{2}$$

with the first (geometric) term is represented by the Einstein tensor, and $T_{\mu\nu}$ represents the total EMT of matter fluid forms. Both $G_{\mu\nu}$ and $T_{\mu\nu}$ are covariantly conserved quantities. The EMT for perfect-fluid models is given by

$$T_{\mu\nu} = (\rho + p)u_\mu u_\nu + p g_{\mu\nu}\,, \tag{3}$$

where ρ and p are the energy density and isotropic pressure of matter, respectively. Related by the barotropic EoS, $p = w\rho$, for a constant EoS parameter w. The normalized vector u_μ represents the four-velocity of fundamental observers moving with the fluid. The divergence-free EMT, $T^{\mu\nu}{}_{;\mu} = 0$ leads to the fluid conservation equation

$$\dot{\rho} + 3\frac{\dot{a}}{a}(1+w)\rho = 0\,, \tag{4}$$

where $a(t)$ is the cosmological scale factor whose evolution is given by the Friedmann equation

$$\frac{\dot{a}^2}{a^2} = \frac{8\pi G}{3}\rho + \frac{\Lambda}{3} - \frac{k}{a^2}\,, \tag{5}$$

where k is the normalized spatial curvature parameter with values $-1\,, 0\,, 1$ depending on an open, flat, or closed spatial geometry, respectively. In our case, we assume a flat spatial geometry.

2.1 Background equations

In a multicomponent fluid system, it is usually assumed that the energy density of each perfect-fluid component evolves independently of the other fluids of the system:

$$\dot{\rho}_i + 3\frac{\dot{a}}{a}(1+w_i)\rho_i = 0\,, \tag{6}$$

and in this case, the EMT in equation (3) is the algebraic sum of the EMTS of each fluid, so are the total energy density and total pressure terms of equation (5) the algebraic sums of the individual components. However, suppose we relax this assumption due to the presence of diffusion between the constituent components of the fluid. In that case, the individual components do not obey the matter conservation equation, but the total fluid still does. For the ith component fluid, the new conservation equation given by (Z. Haba 2010; S. Calogero 2011; D. Benisty et al. 2019) reads:

$$T_i^{\mu\nu}{}_{;\mu} = N_i^\nu\,, \tag{7}$$

where the current of the diffusion term for that fluid, $N_i^\nu = \gamma_i u^\nu$, γ_i represents the number density, and u^μ: $u^\nu u_\nu = -1$ is the four-velocity of the fluids. In the works Z. Haba (2010), S. Calogero (2011, 2012), Z. Haba, A. Stachowski & M. Szydłowski (2016), S. Maity et al. (2019), equation (7) is broadly discussed to express a particular form of interaction between DM and DE. Similar to Z. Haba (2010), we take into account the assumption that the dissipation results from a relativistic motion in a DE fluid. The EMT for DE and DM components of the fluid, the conservation is given as

$$\nabla_\mu T^{\mu\nu}_{\rm de} = -\nabla_\mu T^{\mu\nu}_{\rm dm} = N^\nu = \gamma u^\nu\,.$$

The 00-component of the interaction term reads $N^0 = \gamma/a^3$ for a homogeneous Universe, where the full detail is presented in (Z. Haba et al. 2016). The non-conservation equation for ith fluid can be given by Z. Haba et al. (2016) and S. Maity et al. (2019):

$$\dot{\rho}_i + 3\frac{\dot{a}}{a}(1+w_i)\rho_i = \frac{\gamma_i}{a^3}\,, \quad \text{where } i = b, dm, de, \tag{8}$$

where γ_i is a constant for two dark components that means γ_i stands for $\gamma_{\rm dm}$ and $\gamma_{\rm de}$ for the DM and DE, respectively. The diffusive term vanishes for the baryonic matter $\gamma_{\rm b} = 0$, fluid due to its non-interacting nature. Integrating this equation (8) gives

$$\rho_i = a^{-3(1+w_i)}\left[\rho_{i0} + \gamma_i\int_{t_0}^{t} a^{3w_i}\,\mathrm{d}t'\right]\,, \tag{9}$$

with ρ_{i0} representing the present-day ($t = t_0$) value of the energy density of the ith fluid. Using a late-time $|t - t_0| \ll t_0$ expansion and expressing $a(t) = a_0\,[1 - (t_0 - t)H_0 + \dots]$, we can write the last

term of the above integrand as

$$\begin{aligned}\int_{t_0}^{t} a^{3w_i}\mathrm{d}t &\approx \int_{t_0}^{t} a_0^{3w_i}\left[1-(t_0-t')H_0+\ldots\right]^{3w_i}\mathrm{d}t' \\ &\approx \frac{a_0^{3w_i}}{(1+3w_i)H_0}\Big[(1-(t_0-t)H_0)^{1+3w_i} \\ &\quad -(1+(t_0-t_0)H_0)^{1+3w_i}+\ldots\Big] \\ &\approx \frac{a_0^{3w_i}}{(1+3w_i)H_0}\left[a^{1+3w_i}-1\right]\,. \end{aligned} \tag{10}$$

In the last step, we normalized the scale factor to unity today: $a_0 = 1$. From equations (9) and (10), the energy density of each diffusive fluid component is given according to the relation given below:

$$\rho_i \approx a^{-3(1+w_i)}\left[\rho_{i0}+\frac{\gamma_i}{(1+3w_i)H_0}\left(a^{1+3w_i}-1\right)\right]\,. \tag{11}$$

Assuming the well-known component of radiation is negligible,[2] the energy density of dust-like matter $\rho_m = \rho_b + \rho_{\rm dm}$ for the case of baryons and DM, and the corresponding EoS parameter, $w_{\rm m} = w_{\rm b} = w_{\rm dm} = 0$. For the case of vacuum energy, we consider $p_{\rm de} = w_{\rm de}\rho_{\rm de}$, where the EoS parameter is $w_{\rm de} = -1$. The above diffusive solution leads to:

$$\rho_{\rm m} = a^{-3}\left[\rho_{\rm m0}+\frac{\gamma_{\rm dm}}{H_0}(a-1)\right]\,,\ \text{since}\ \ \rho_{\rm m0} = \rho_{\rm b0}+\rho_{\rm dm0} \tag{12}$$

and

$$\rho_{\rm de} = \rho_{\rm de0}-\frac{\gamma_{\rm de}}{2H_0}\left(a^{-2}-1\right)\,. \tag{13}$$

It is worth mentioning at this point that the DM energy density $\rho_{\rm dm}$ no longer scales like a^{-3} since the extra items. This equation can be rewritten in a way that resembles the DM scaling equation provided in K. Naidoo et al. (2024), according to which we can expect a change in the Integrated Sachs–Wolfe (ISW) effect. The modified Friedmann equation due to the presence of the diffusive dark fluid is given by

$$\begin{aligned}H^2 = \frac{8\pi G}{3c^4}\Big[&\rho_{\rm m0}a^{-3}+\frac{\gamma_{\rm dm}}{H_0}(a-1)\,a^{-3} \\ &+\rho_{\rm de0}-\frac{\gamma_{\rm de}}{2H_0}\left(a^{-2}-1\right)\Big]. \end{aligned} \tag{14}$$

Here, we introduce the following dimensionless dynamical quantities:

$$\Omega_i \equiv \frac{8\pi G}{3H_0^2}\rho_i\,,\ Q_{\rm dm} \equiv \frac{8\pi G}{3H_0^3}\gamma_{\rm dm}\,,\ Q_{\rm de} \equiv \frac{8\pi G}{3H_0^3}\gamma_{\rm de}\,,\ h \equiv \frac{H(z)}{H_0}\,.$$

Then, the normalized Hubble parameter yields[3]

$$h^2(z) = \Omega_{\rm m}(1+z)^3+\Omega_{\rm de}-Q_{\rm dm}(1+z)^2 z-\frac{1}{2}Q_{\rm de}(z^2+2z). \tag{15}$$

In this work, we assume that the interaction exists only between the dark components and given the requirement $\sum\gamma_i = 0$ for total energy conservation. Hereafter, we set $Q_{\rm de} = -Q_{\rm dm}$. From equation (15), the simplified form of the deceleration parameter is yielded as

$$q(z) = -1+\frac{(1+z)^2\left(3\Omega_{\rm m}(1+z)-3zQ_{\rm dm}\right)}{2\left(\Omega_{\rm m}(1+z)^3+\Omega_{\rm de}-\frac{1}{3}Q_{\rm dm}z^2-Q_{\rm dm}z^3\right)}. \tag{16}$$

Then, the corresponding effective EoS parameter ($w_{\rm eff}$) for the diffusive dark fluid is obtained as

$$w_{\rm eff}(z) = -\frac{1}{3}+\frac{2}{3}q(z)\,. \tag{17}$$

Using equation (15), it is straightforward to compute the cosmological distance measures such as the distance modulus $\mu(z)$, which is given by

$$\mu(z) = 25+5\log_{10}D_{\rm L}(z)\,, \tag{18}$$

where $D_{\rm L}(z)$ is the luminosity distance. It is given by

$$D_{\rm L}(z) = (1+z)300\bar{h}^{-1}\int_0^z\frac{c\mathrm{d}z'}{h(z')'}\,. \tag{19}$$

Here, $\bar{h} = H_0/100$, and $D_{\rm L}(z)$ is measured in Mpc. The volume-averaged angular diameter distance reflects BAO measurements averaged over spherical distances.

$$D_{\rm V}(z) = \left[(1+z)^2 D_{\rm A}^2(z)^2\frac{300\bar{h}^{-1}z}{h(z)}\right]^{\frac{1}{3}}\,, \tag{20}$$

and the angular distance yields

$$D_{\rm A}(z) = \frac{\bar{h}^{-1}}{(1+z)}\int_0^z\frac{\mathrm{d}z'}{h(z')}\,. \tag{21}$$

The sound horizon at the drag $r_{\rm d}$ epoch is given by

$$r_{\rm d} = \int_{z_{\rm d}}^{\infty}\frac{c_{\rm s}(z)}{H(z)}\mathrm{d}z\,, \tag{22}$$

where $z_{\rm d}$ is the redshift at drag epoch and $c_{\rm s}(z)$ is the sound speed of the photon-baryon fluid.

2.2 Perturbation equations

In this section, we apply the 1+3 covariant gauge-invariant perturbation formalism to study the structure formation within the framework of diffusive dark-fluid cosmology. The $1+3$ covariant formalism decomposes space–time into temporal and spatial components using the observer's four-velocity $u^a = \frac{\mathrm{d}x^a}{\mathrm{d}\tau}$, where x^a denotes the coordinates and τ is the proper time. This approach helps to analyse crucial quantities such as the rate of fluid (volume) expansion ($\Theta \equiv \tilde{\nabla}_a u^a = 3\mathrm{H}$), shear ($\sigma_{ab} = \sigma_{(ab)}$), and vorticity ($\omega_{ab} = \omega_{[ab]}$). The Raychaudhuri equation governs the dynamics of expansion in a cosmological setting and plays a crucial role in understanding the formation of singularities; it is given by:

$$\dot{\Theta} = -\frac{1}{3}\Theta^2-\sigma_{ab}\sigma^{ab}+\omega_{ab}\omega^{ab}-R_{ab}u^a u^b+\tilde{\nabla}^a\dot{u}_a\,, \tag{23}$$

where, R_{ab} is the Ricci curvature tensor, indicating the curvature of space–time due to gravitational effects, and $R_{ab}u^a u^b = \frac{1}{2}\kappa(1+3w)\rho$ (G. Ellis et al. 1990; P. Dunsby et al. 1992), where $\kappa \equiv \frac{8\pi G}{c^4}$. In our case, we assume shear-free $\sigma_{ab} = 0$, and free rotational $\omega_{ab} = 0$ space–time, and the Raychaudhuri equation is reduced to

$$\dot{\Theta} = -\frac{1}{3}\Theta^2-\frac{1}{2}\kappa(1+3w)\rho+\tilde{\nabla}^a\dot{u}_a\,. \tag{24}$$

To simplify the structure formation, we assume that adiabatic perturbations where the EoS parameter is constant $\dot{w} = 0$. To begin traditionally, we start by defining the gradient variables describing

[2]Since the contribution of radiation to the late-time cosmological expansion history is so minimal, we have safely neglected such a contribution in the analysis to be performed.
[3]Note that the matter density parameter is $\Omega_{\rm m} = \Omega_{\rm b}+\Omega_{\rm dm}$.

the fluctuations (G. F. Ellis & M. Bruni 1989b; G. Ellis et al. 1990; P. Dunsby et al. 1992; G. F. Ellis & H. Van Elst) in the individual energy densities ($i = m, \Lambda$) and the volume expansion as

$$D_a^i \equiv \frac{a\tilde{\nabla}_a \rho_i}{\rho_i}\ , \quad Z_a \equiv a\tilde{\nabla}_a \Theta\ , \tag{25}$$

where the tilde nabla operator $\tilde{\nabla}$ denotes the spatially projected covariant derivative. These gradient variables evolve according to the following equations:

$$\dot{D}_a^i = -(1+w_i)Z_a + \left[\frac{w_{\rm m}(1+w_i)\Theta\rho_i}{(1+w_{\rm m})\rho_{\rm m}} + \left(\frac{w_{\rm m}}{(1+w_{\rm m})\rho_{\rm m}} + \frac{1}{\rho_i}\right)\gamma_i a^{-3}\right] D_a^i\ , \tag{26}$$

$$\dot{Z}_a = -\frac{2}{3}\Theta Z_a - \left[\frac{1+3w_{\rm m}}{2} + \frac{w_{\rm m}}{(1+w_{\rm m})}\tilde{\nabla}^2\right]\rho_{\rm m} D_a^{\rm m} - \rho_\Lambda D_a^\Lambda\ . \tag{27}$$

By setting the EoS parameter $w_{\rm m} = 0$ for DM and $w_{\rm de} = -1$ for DE, the corresponding system of first-order evolution equations yields:

$$\dot{D}_a^{\rm m} + Z_a - \frac{1}{\rho_{\rm m}}\gamma_{\rm dm} a^{-3} D_a^{\rm m} = 0, \tag{28}$$

$$\dot{D}_a^{\rm de} - \frac{1}{\rho_{\rm de}}\gamma_{\rm de} a^{-3} D_a^{\rm de} = 0, \tag{29}$$

$$\dot{Z}_a + \frac{2}{3}\Theta Z_a + \frac{1}{2}\rho_{\rm m} D_a^{\rm m} + \rho_{\rm de} D_a^\Lambda = 0. \tag{30}$$

We followed the following steps to get the evolution equations of density fluctuations from equations (28) and (29). In the first case, we take into account the second-order time-dependent evolution equations from equations (28) and (29). In the second case, we implement the scalar decomposition technique developed originally by the work in G. F. Ellis & M. Bruni (1989b), P. Dunsby et al. (1992), and A. Abebe et al. (2012a) to extract any scalar variable Y using the relation $a\nabla_a Y_b = Y_{ab} = \frac{1}{3}h_{ab}Y + \Sigma_{ab}^Y + Y_{[ab]}$. Here $Y = a\nabla_a Y^a$, whereas $\Sigma_{ab}^Y = Y_{(ab)} - \frac{1}{3}h_{ab}Y$ and $Y_{[ab]}$ represent the shear (distortion) and vorticity (rotation) of the density gradient field, respectively. Then, we define the following scalar quantities as G. F. Ellis & M. Bruni (1989b), P. Dunsby et al. (1992), A. Abebe et al. (2012a, 2013), J. Ntahompagaze et al. (2018), S. Sahlu et al. (2020, 2025b), H. Sami et al. (2021)

$$\Delta_i = a\tilde{\nabla}^a D_a^i\ , \quad \text{and} \quad Z = a\tilde{\nabla}^a Z_a, \tag{31}$$

where i stands for matter and DE components. In the third step, we shall pay attention to solving the density contrast by resorting to the evolution equations (31), and we use the initial values of the system given by S. Sahlu et al. (2020, 2024, 2025a, b)

$$\delta_i(z) = \frac{\Delta_i(z)}{\Delta_i(z_{\rm in})}\ , \tag{32}$$

where the subscript in refers to the initial value of $\Delta_i(z)$ at the given initial redshift $z_{\rm in}$.

Finally, we transformed the time-dependent to redshift space as presented in S. Sahlu et al. (2020, 2024, 2025b) and H. Sami et al. (2021) after following the scalar decomposition technique mentioned in the above second case.[4] Then the coupled second-order system of equations in redshift space becomes

$$(1+z)^2\delta_{\rm m}'' + \left[(1+z)^2\frac{h'}{h} - (1+z) + \frac{Q_{\rm dm}}{\Omega_{\rm m}}\frac{1}{h}\right]\delta_{\rm m}' + \frac{1}{h^2}\left[\frac{Q_{\rm dm}^2}{\Omega_{\rm m}^2}(1+z)^6 - \frac{2Q_{\rm dm}}{\Omega_{\rm m}}(1+z)^3 h - \frac{3\Omega_{\rm m}}{2}(1+z)^3\right]\delta_{\rm m} + - 3\Omega_{\rm de}\delta_{\rm de} = 0, \tag{33}$$

$$(1+z)^2\delta_{\rm de}'' + \left[(1+z)^2\frac{h'}{h} + (1+z) - \frac{Q_{\rm dm}}{\Omega_{\rm de}}(1+z)^4\frac{1}{h}\right]\delta_{\rm de}' - \frac{1}{h^2}\left[\frac{Q_{\rm dm}^2}{\Omega_{\rm de}^2}(1+z)^6 - 3\frac{Q_{\rm dm}}{\Omega_{\rm de}}(1+z)^3 h\right]\delta_{\rm de} = 0, \tag{34}$$

where $'$ and $''$ represent the first- and second-order derivatives with respect to the redshift, z. This coupled system of equations (33) and (34) indicates that the cosmological perturbation of DE is not identically zero, and further study has been found in the work (J.-H. He, B. Wang & Y. Jing 2009), where the influence of non-vanishing DE perturbations is considered. The numerical results of these coupled system equations are presented later in Section 3.4, and the result is strongly favoured for the $\delta_{\rm m} \gg \delta_{\rm de}$. Hereafter, we extended further investigations of the large-scale structure by considering the assumption $\delta_{\rm m}(z) \gg \delta_{\rm de}(z)$, that the DM component makes a significant contribution to structure formation. Without DM, the structure formation would not have enough time to grow. By admitting this assumption, we have a closed system of evolution equations from equation (33), and it is given as

$$(1+z)^2\delta_{\rm m}'' + \left[(1+z)^2\frac{h'}{h} - (1+z) + \frac{Q_{\rm dm}}{\Omega_{\rm m}}\frac{1}{h}\right]\delta_{\rm m}' + \frac{1}{h^2}\left[\frac{Q_{\rm dm}^2}{\Omega_{\rm m}^2}(1+z)^6 - \frac{2Q_{\rm dm}}{\Omega_{\rm m}}(1+z)^3 h - \frac{3\Omega_{\rm m}}{2}(1+z)^3\right]\delta_{\rm m} = 0. \tag{35}$$

The diffusive dark-fluid model treats the dark sector as a single fluid with energy exchange between DM and DE, influencing the evolution of cosmological perturbations and potentially altering the growth of cosmic structures compared to the standard ΛCDM model (K. Naidoo et al. 2024). The diffusive model's damping effect affects matter distribution and leaves observable imprints on the CMB, providing an alternative explanation for the Universe's accelerated expansion that can be tested through galaxy surveys and observations of structure growth. The normalized density contrast $\delta_{\rm m}(z)$, plays a key role in the formation of cosmic structures. It starts small, growing through gravitational instability to form galaxies and clusters. Afterward, we have considered the growth factor $D(z)$ that represents the ratio of the amplitude of $\delta_{\rm m}(z)$ in redshift z compared to an initial value $\delta_{\rm m}(z=0)$ becomes

$$D(z) = \frac{\delta_{\rm m}(z)}{\delta_{\rm m}(z=0)}\ . \tag{36}$$

It is often normalized to $\delta(z=0) = 1$ and is governed by a differential equation that involves the Hubble parameter the density of matter. This factor shows how initial density perturbations grow over time due to gravity, influencing the formation of large-scale structures. In a DE-dominated Universe, the growth slows due to accelerated expansion. The growth factor is crucial for modelling galaxy formation and comparing theoretical predictions with observations, such as those from the CMB and galaxy surveys (V. Springel et al. 2006). Additionally, the growth rate $f(z)$, related to $D(z)$, measures structure growth and is used in observational probes such as redshift-space distortions $f\sigma_8$. From equation (36), the growth

[4] We consider a similar manner as Ref. in P. Louis et al. (2019), which neglects the scale dependence, and the density contrast is rewritten as $\delta(k, z) = \delta(z)$.

rate $f(z)$ is yields as

$$f \equiv \frac{\mathrm{d}\ln D}{\mathrm{d}\ln a} = -(1+z)\frac{\delta'_{\rm m}(z)}{\delta_{\rm m}(z)}\,. \tag{37}$$

Therefore, the growth factor is fundamental to understanding the dynamical evolution of the structures of the universe. Thus, substituting the definition of (37) into the second-order evolution equation (36), the growth rate is governed by

$$(1+z)f' = f^2 - \left((1+z)\frac{h'}{h} - 2 + \frac{Q_{\rm dm}}{\Omega_{\rm m}}\frac{1}{h(1+z)}\right) f$$
$$-\frac{1}{h^2}\left(\frac{Q_{\rm dm}^2}{\Omega_{\rm m}^2}(1+z)^6 - \frac{2Q_{\rm dm}}{\Omega_{\rm m}}(1+z)^3 h - \frac{3\Omega_{\rm m}}{2}(1+z)^3\right). \tag{38}$$

For the case of $Q_{\rm dm} = 0$, the evolution equation of the density fluctuation for ΛCDM is recovered. A combination of the linear growth rate $f(z)$ with the root-mean-square normalization of the matter power spectrum σ_8 within the radius sphere $8h^{-1}$Mpc, yields the redshift-space distortion $f\sigma_8$ A. Hamilton (1998) as

$$f\sigma_8(z) = -(1+z)\sigma_8\frac{\delta'_{\rm m}(z)}{\delta_{\rm m}(z)}\,. \tag{39}$$

Note that all the above background and perturbation evolution equations are reduced to the ΛCDM model for the closure of vanishing interaction term, $Q_{\rm dm} = 0$. In the subsequent section, as presented in 3.1, we emphasize the matter clustering S_8 that is given by

$$S_8 = \sigma_8\sqrt{\frac{\Omega_{\rm m}}{0.3}}\,,$$

to explain the viability of the diffusive model to explain the cosmic structure growth and matter distribution in the Universe.

3 RESULTS AND DISCUSSION

Using the recent cosmological measurements, this section gives a detailed analysis of the constraining parameters, the comparison of H_0 (in km s^{-1} Mpc^{-1}) and S_8 values with different cosmological surveys, the numerical result of background cosmological parameters, structure growth, and statistical analysis that show the implications of the diffusive model against the ΛCDM model.

3.1 Constraining parameters

We consider the PYTHON libraries, including EMCEE (D. Foreman-Mackey et al. 2013; R. Hough et al. 2020) and GetDist (A. Lewis 2019), to constrain the values of the parameters using the mentioned in the below cosmological measurements. We have considered the following recent cosmological measurements to constrain the model parameters:

(i) *BAO*: The BAO distance and the correlation measurements released data 2 (DR2; M. Abdul-Karim et al. 2025; U. Andrade et al. 2025) from the Dark Energy Spectroscopic Instrument (DESI) Survey have been considered. The measurements include data for the isotropic BAO measurements of $D_{\rm V}(z)/r_{\rm d}$, where $D_{\rm V}(z)$ and $r_{\rm d}$ are the spherically averaged volume distance and sound horizon at baryon drag, respectively. And anisotropic BAO measurements of $D_{\rm M}(z)/r_{\rm d}$ and $D_{\rm H}(z)/r_{\rm d}$, where $D_{\rm M}(z)$ and $D_{\rm H}(z)$ are the co-moving angular diameter distance and the Hubble distance, respectively, and the correlations between the isotropic and anisotropic BAO measurements. Hereafter, we refer to this data set as *DESI DR2 BAO*.

(ii) *Supernovae Type Ia (SNIa)* data set compilations we have considered the following, namely: (i) *PPS:* we use the SNIa distance moduli measurements from the Pantheon+ sample (D. Brout et al. 2022), which consists of 1701 light curves of 1550 distinct SNIa ranging in the redshift interval $z \in [0.001, 2.26]$, (ii) *DESY5* data (R. Chiba & T. J. Moriya 2024) which is a photometrically-classified SNIa with redshifts in the range $0.1 < z < 1.13$, complemented by 194 historical low-redshift SNe Ia (which are also present in the PPS sample) spanning $0.025 < z < 0.1$, (iii) *Union3* we have consider the up-to-date Union compilation of 2087 cosmologically useful SNIa from 24 data sets (D. Rubin et al. 2025).

(iii) *Cosmic chronometers*: We analyse the Hubble parameter $H(z)$ measurements with observational Hubble parameter data. This comprises 31 data points derived from the relative ages of massive, early-time, passively evolving galaxies, known as cosmic chronometers (CC). We refer to this data set as CC. We calculate the minimum χ^2 with CC covariance in combination with statistical and systematic effects as presented in chronometers (CC) (M. Moresco et al. 2020; J.-Z. Qi et al. 2023)

$$\chi^2_{\rm CC} = (H_{\rm theo}(z) - H_{\rm ob}(z_i))^T\, C^{-1}\, (H_{\rm theo}(z) - H_{\rm ob}(z_i))\,,$$

where $H_{\rm theo}(z)$ represents the theoretical model of the Hubble parameter and $H_{\rm ob}(z_i)$ the Hubble parameter measurement.

(iv) *Large scale structure*: We also incorporate RSD and the growth rate, labelled RSD, from the VIPERS and SDSS collaborations. (i) A total of 66 data points of the measurements of redshift-space distortion for $f\sigma_8$ have been collected and summarized in the works of L. Kazantzidis & L. Perivolaropoulos (2018) and F. Skara & L. Perivolaropoulos (2020), covering the redshift interval $0.001 \leq z \leq 1.944$. (ii) 14 growth rate f data points within the redshift range $0.001 \leq z \leq 1.4$ (A. Woodfinden et al. 2022). The resulting χ^2 for redshift-space distortion and growth rate are expressed as:

$$\chi^2_{\rm RSD} = \left(f\sigma_{8,\rm theo} - f\sigma_{8,\rm ob}(z_i)\right)^T C^{-1} \left(f\sigma_{8,\rm theo} - f\sigma_{8,\rm ob}(z_i)\right)\,,$$

and

$$\chi^2_f = (f_{\rm theo} - f_{\rm ob}(z_i))^T\, C^{-1}\, (f_{\rm theo} - f_{\rm ob}(z_i))\,,$$

respectively.

(v) *Joint data sets*: The combined data analysis improves the precision and constraints on the models we employ, allowing for a more complete picture of the Universe. By considering the inconsistency of the *PPS* & DESI *BAO* data sets as presented in the S. Afroz & S. Mukherjee (2025) disclosed through a violation of the distance duality relation, we have considered a joint analysis

(a) *PPS + CC + DESY5 + RSD + f*
(b) *DESI DR2 BAO + CC + Union3 + RSD + f* and
(c) *DESI DR2 BAO + CC + DESY5 + Union3 + RSD f*

for both theoretical models. The corresponding χ^2 is given by

$$\chi^2_{\rm tot} = \sum_k \chi^2_k\,,$$

where k stands for *DES BAO, PPS, CC, DESY5, Union3, RSD*, and *f*.

In the present work, we have emphasized the above two joint data sets to constrain the cosmological parameters $h, \Omega_{\rm m}$, $Q_{\rm dm}$, $r_{\rm d}$, M, and σ_8, and for detailed statistical analysis, see Table 1. The values of our constrained parameters are highly sensitive to the prior on $Q_{\rm dm}$, and we have set the following priors: $\Omega_{\rm m} = [0.1, 1.0]$, $H_0 = [0.0, 1.0]$, $r_{\rm d} = [100, 200]$, $Q_{\rm dm} = [-0.05, 0.05]$, and$M = [-15.00, 22.00]$. We present the posterior

Table 1. Marginalized 68 per cent and 95 per cent confidence level (C.L) limits of the parameters in the data set combinations for the diffusive model and the ΛCDM model.

Parameter	C.L	*PPS + CC + DESY5 + RSD + f*	*DESI DR2 BAO + CC + Union3 + RSD + f*	*DESI DR2 BAO + CC + DESY5 Union3 + RSD + f*
Diffusive model				
H_0 (km s^{-1} Mpc^{-1})	68 per cent	$68.959^{+0.193}_{-0.193}$	$69.469^{+0.169}_{-0.169}$	$69.465^{+1.392}_{-1.385}$
	95 per cent	$68.959^{+0.378}_{-0.377}$	$69.469^{+0.333}_{-0.333}$	$69.465^{+2.761}_{-2.730}$
	Best fit	68.959	69.469	69.465
Ω_m	68 per cent	$0.361^{+0.009}_{-0.009}$	$0.331^{+0.007}_{-0.007}$	$0.309^{+0.008}_{-0.007}$
	95 per cent	$0.361^{+0.017}_{-0.017}$	$0.331^{+0.013}_{-0.013}$	$0.309^{+0.015}_{-0.014}$
	Best fit	0.361	0.331	0.309
r_d	68 per cent	–	$142.239^{+0.649}_{-0.644}$	$144.726^{+2.920}_{-2.808}$
	95 per cent	–	$142.239^{+1.278}_{-1.269}$	$144.726^{+5.873}_{-5.463}$
	Best fit	–	142.239	144.726
Q_{dm}	68 per cent	$-0.013^{+0.002}_{-0.002}$	$-0.007^{+0.001}_{-0.001}$	$-0.004^{+0.001}_{-0.001}$
	95 per cent	$-0.013^{+0.004}_{-0.004}$	$-0.007^{+0.003}_{-0.003}$	$-0.004^{+0.003}_{-0.003}$
	Best fit	−0.013	−0.007	−0.004
M	68 per cent	$-19.373^{+0.005}_{-0.005}$	–	–
	95 per cent	$-19.373^{+0.011}_{-0.011}$	–	–
	Best fit	−19.373	–	–
σ_8	68 per cent	$0.788^{+0.019}_{-0.019}$	$0.771^{+0.019}_{-0.018}$	$0.756^{+0.018}_{-0.018}$
	95 per cent	$0.788^{+0.038}_{-0.037}$	$0.771^{+0.037}_{-0.036}$	$0.756^{+0.036}_{-0.035}$
	Best fit	0.788	0.767	
S_8	68 per cent	$0.864^{+0.027}_{-0.026}$	$0.809^{+0.023}_{-0.022}$	$0.766^{+0.023}_{-0.023}$
	95 per cent	$0.864^{+0.053}_{-0.050}$	$0.809^{+0.046}_{-0.044}$	$0.766^{+0.046}_{-0.044}$
Best fit		0.864	0.809	0.766
ΛCDM model				
H_0	68 per cent	$69.950^{+0.146}_{-0.147}$	$69.968^{+0.143}_{-0.143}$	$70.101^{+1.386}_{-1.372}$
	95 per cent	$69.950^{+0.287}_{-0.288}$	$69.968^{+0.282}_{-0.281}$	$70.101^{+2.753}_{-2.700}$
	Best fit	69.950	69.968	70.101
Ω_m	68 per cent	$0.310^{+0.005}_{-0.005}$	$0.306^{+0.005}_{-0.004}$	$0.293^{+0.005}_{-0.005}$
	95 per cent	$0.310^{+0.010}_{-0.010}$	$0.306^{+0.009}_{-0.009}$	$0.293^{+0.009}_{-0.009}$
	Best fit	0.310	0.306	0.293
r_d	68 per cent	–	$144.197^{+0.560}_{-0.560}$	$145.369^{+2.923}_{-2.831}$
	95 per cent	–	$144.197^{+1.109}_{-1.099}$	$145.369^{+5.861}_{-5.504}$
	Best fit	–	144.197	145.369
M	68 per cent	$-19.359^{+0.005}_{-0.005}$	–	
	95 per cent	$-19.359^{+0.010}_{-0.010}$	–	
	Best fit	−19.359	–	
σ_8	68 per cent	$0.805^{+0.018}_{-0.018}$	$0.796^{+0.018}_{-0.017}$	$0.765^{+0.018}_{-0.017}$
	95 per cent	$0.805^{+0.036}_{-0.035}$	$0.796^{+0.035}_{-0.034}$	$0.765^{+0.035}_{-0.034}$
	Best fit	0.805	0.796	0.765
S_8	68 per cent	$0.818^{+0.023}_{-0.023}$	$0.804^{+0.022}_{-0.021}$	$0.756^{+0.022}_{-0.021}$
	95 per cent	$0.818^{+0.046}_{-0.045}$	$0.804^{+0.044}_{-0.042}$	$0.756^{+0.044}_{-0.042}$
	Best fit	0.818	0.804	0.756

distributions of these parameters in Figs 1, 2, and 3 for the ΛCDM and diffusive model, respectively. The parameter values are summarized in the marginalized 68 per cent and 95 per cent confidence limits in Table 1 for joint data sets, *PPS + CC + DESY5 + RSD + f*, *DESI DR2 BAO + CC + DESY5 + RSD + f*, and *DESI DR2 BAO + CC + Union3 + RSD + f*. We notice that the value of the interaction term is negative, see the best-fitting values in Table 1, $Q_{dm} = -0.013,\ -0.007,\ -0.004$ at 68 per cent and 95 per cent C.Ls for the considered joint data sets. This indicates a case where energy flows from DM to DE, driving the Universe's accelerating expansion,

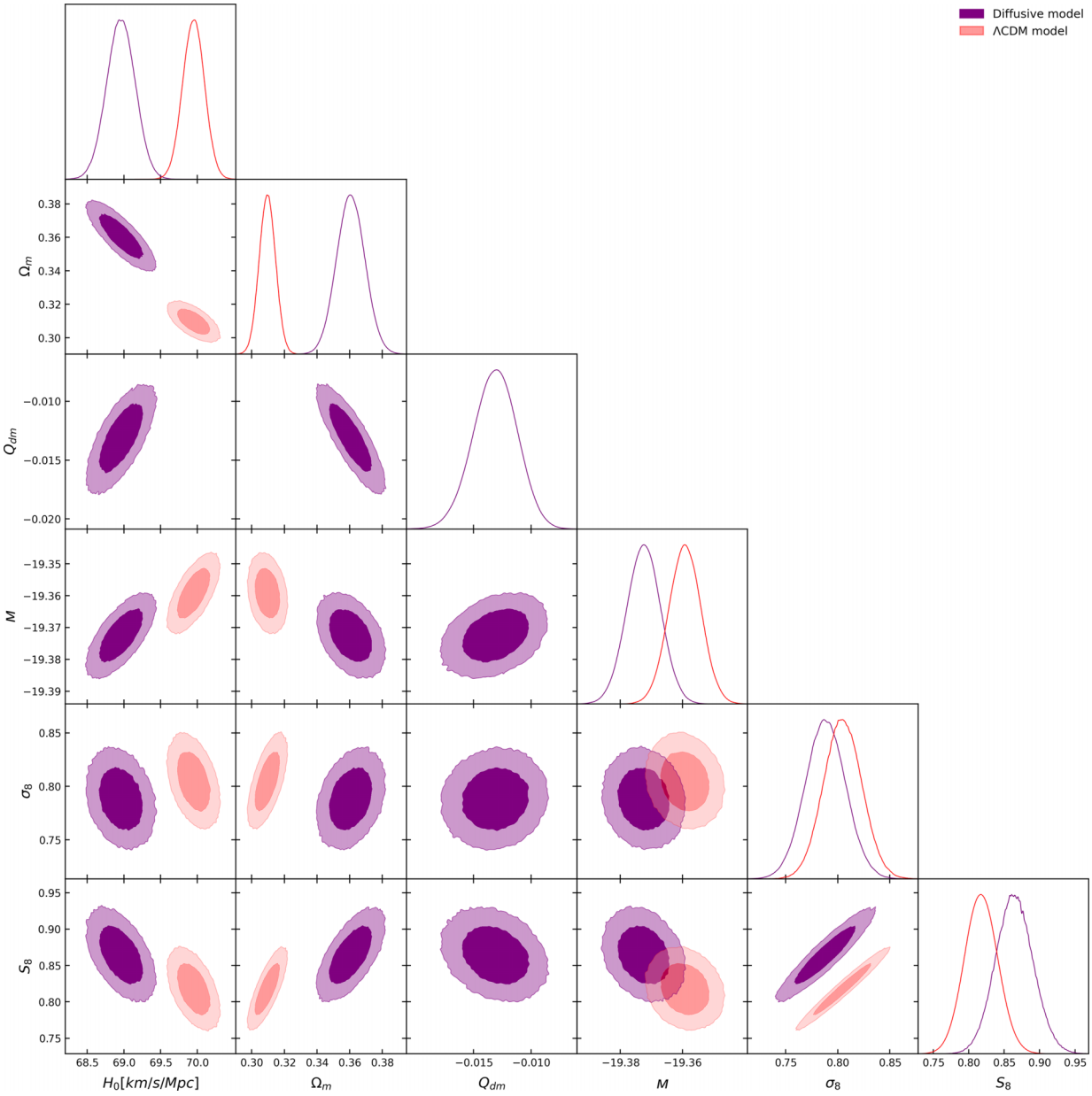

Figure 1. Posterior distributions of the parameters using $PPS + CC + DESY5 + RSD + f$ for both models.

as supported by recent observational evidence (D. Benisty et al. 2019; E. Silva et al. 2025; M. Westhuizen et al. 2025). In the subsequent sections, we shall choose 95 per cent of C.L of the values of the interacting term $Q_{\rm dm} = -0.013^{+0.004}_{-0.004} = -0.017, -0.013, -0.009$ as listed in Table 1 to show our numerical results.

From the constrained parameters presented in the Table. 1 and Figs 1, the diffusive model has slightly lower values of H_0 ($\rm km\,s^{-1}\,Mpc^{-1}$) and σ_8 but higher values of $\Omega_{\rm m}$ introducing $\Omega_{\rm m}$ tension compared with ΛCDM model which leads to the slightly higher deviation of the values S_8 between both models. This deviation is significantly noticed for $PPS + CC + DESY5 + RSD + f$ data sets, where the best-fitting values of $\Omega_{\rm m} = 0.361$ for the diffusive model, which leads to S_8 tension. For instance, at 95 per cent confidence level the value of the density parameter $\Omega_{\rm m} = 0.361^{+0.017}_{-0.017}$ which is higher in the diffusive model than the $0.310^{+0.010}_{-0.010}$ in the ΛCDM model (see Table. 1). The deference is by 2.6σ which is a significant deviations. Similarly, this deviation is 2.3σ when comparing the diffusive model (using the same $\Omega_{\rm m}$ value) to Planck's measured $\Omega_{\rm m} = 0.315 \pm 0.01$ (N. Aghanim et al. 2020). Notably, these tensions are significantly alleviated when considering data combinations involving DESI DR2 with CC, DESY5, and Union3, as presented in Table 1 and Figs 2 and 3.

Indeed, the increased precision in Hubble parameter ($H_0\,\rm km\,s^{-1}\,Mpc^{-1}$) measurements indicates a disparity between indirect and direct measurements in estimating the present-day expansion rate of the Universe, known as the Hubble tension (A. G. Riess et al. 2011, 2019, 2022; L. Verde et al. 2019; N. Aghanim et al. 2020; K. C. Wong et al. 2020; E. Di Valentino 2021; A. Adame et al. 2025). Besides, the discrepancy in the inferred value of the matter clustering parameter has been reported based on the observations of Planck-2018, KiDS-1000 (H. Hildebrandt et al. 2017), KiDS-450 (M. Asgari et al. 2021) DES Y1 (T. M.

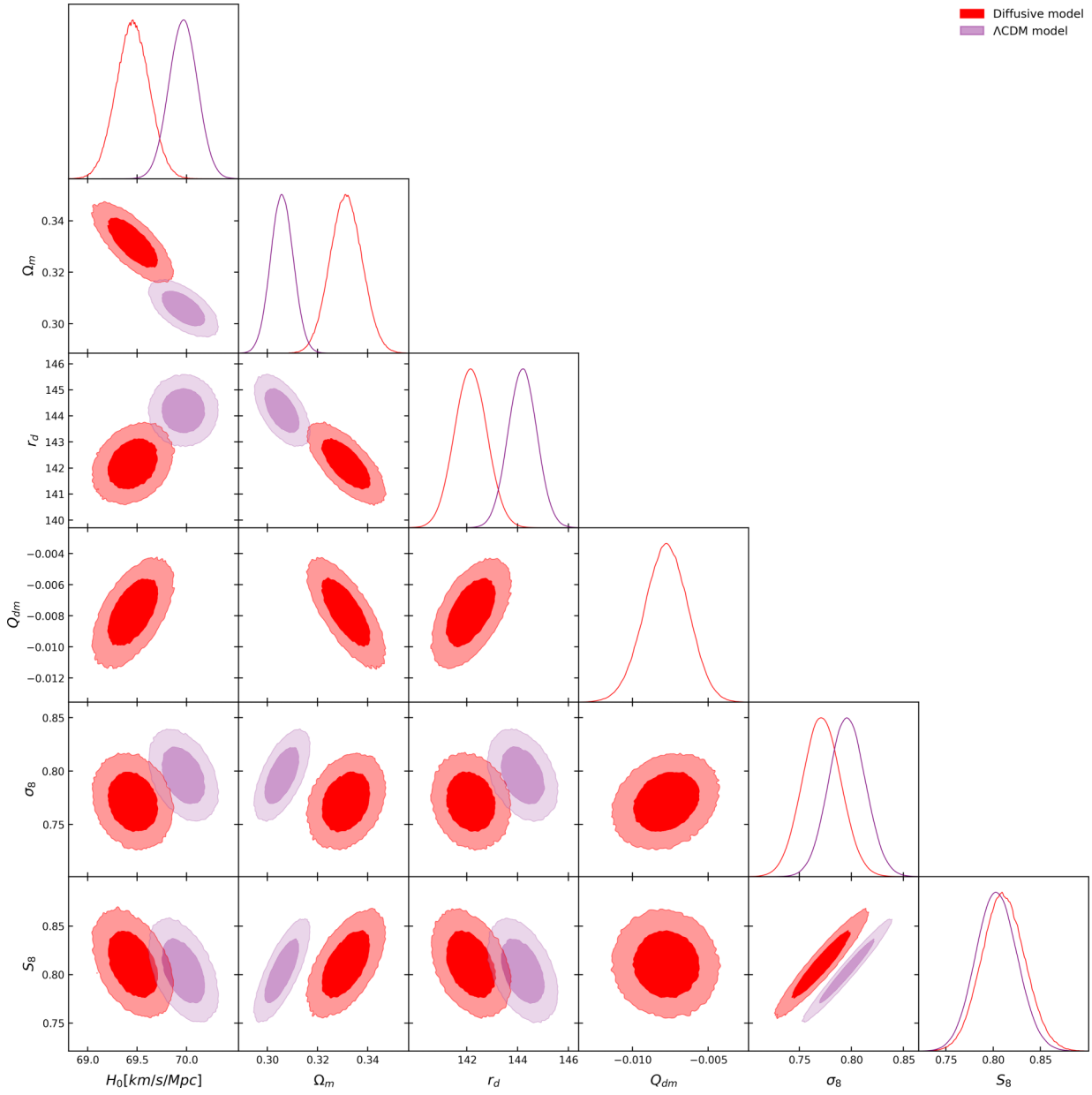

Figure 2. Posterior distributions of the parameters using *DESI DR2 BAO* + *CC* + *DESY5* + *RSD* + f for both models.

Abbott et al. 2018), DES Y3 (A. Amon et al. 2022), and $f\sigma_8(z)$ measurements from RSD mentioned a few. Unlike the discrepancy, measurements of H_0 ($\mathrm{km\,s^{-1}\,Mpc^{-1}}$) and S_8 remain unresolved, providing new cosmological insights beyond the ΛCDM model (E. Di Valentino et al.). In this section, we compare the H_0 ($\mathrm{km\,s^{-1}\,Mpc^{-1}}$) and S_8 values of the diffusive model to those of the ΛCDM model alongside various measurements, indicating that the diffusive model gained the capability to mitigate cosmological tensions. To do that, we first shall take into consideration the H_0 measurements with (i) the indirect measurements, including Planck 2018 ($H_0 = 67.4 \pm 0.5\,\mathrm{km\,s^{-1}\,Mpc^{-1}}$) (N. Aghanim et al. 2020), DESI-2024 ($H_0 = 68.52 \pm 0.62\,\mathrm{km\,s^{-1}\,Mpc^{-1}}$) (A. Adame et al. 2025); and (ii) the direct measurements derived from direct observations of the local Universe, such as Supernovae and H_0 for SH0ES ($H_0 = 74.03 \pm 1.42$) (A. G. Riess et al. 2019), H0LiCOW ($H_0 = 73.3 \pm 1.8$) (K. C. Wong et al. 2020), and *Hubble Space Telescope* ($H_0 = 73.8 \pm 2.4\,\mathrm{km\,s^{-1}\,Mpc^{-1}}$) (A. G. Riess et al. 2011). For instance, the deviation between the SNIa (SH0ES) and Planck 2018 measurements of H_0 is 5.28σ. From the results in Table 1, the diffusive model's $H_0 = 100h$ values (the 95 per cent C.L considered) for the data sets *PPS* + *CC* + *DESY5* + *RSD* + f, *DESI DR2 BAO* + *CC* + *DESY5* + *RSD* + f, and *DESI DR2 BAO* + *CC* + *Union3* + *RSD* + f differ from the Planck 2018 measurement by 2.49σ, 3.44σ, and 0.74σ, respectively. Similarly, the diffusive model differ from SNIa (SH0ES) by -3.45σ, -3.12σ, and -1.48σ for the same data sets, respectively. *Note that, the negative sign in the sigma difference represent the measured value's is higher than the hypothetical model's values.* The corresponding differences between the ΛCDM H_0 values (from the same table) and the Planck measurement increase to 4.42σ, 4.47σ, and 0.94σ, respectively. In the same manner, differences between the ΛCDM H_0 values and SNIa (SH0ES) is -2.81σ, -2.80σ, and -1.28σ. All

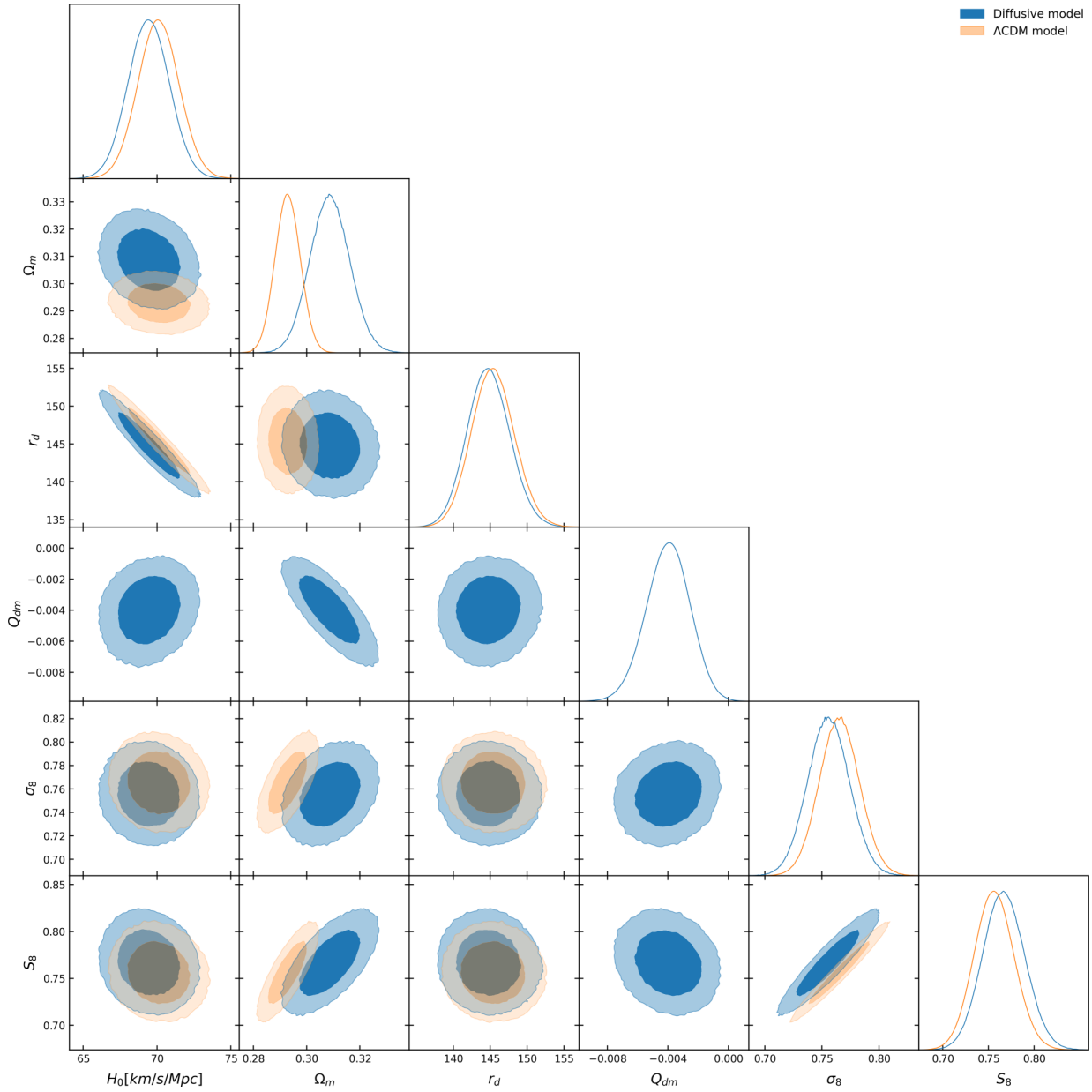

Figure 3. Posterior distributions of the parameters using *DESI DR2 BAO* + *CC* + *Union3* + *RSD* + *f* for both models.

these values of H_0 in $\mathrm{km\,s^{-1}\,Mpc^{-1}}$ are presented in Fig. 4 (left panel) together with the direct and indirect measurements. From this Figure and above mentioned sigma compression, we notice that the diffusive model favoured to indirect measurements while the ΛCDM model is favoured by the direct measurements. Overall, diffusive model show smaller sigma differences compared with the 5.28σ tension and thus partially relax the tension, which requires further investigation.

Secondly, we pay attention to matter clustering S_8, a critical cosmological measure that evaluates the growth of structure in the Universe. The observational tension between CMB and large-scale structure surveys may hint at novel physics beyond the ΛCDM model. We constrain the S_8 results in Fig. 4 (right-panel) for both theoretical models using the above-mentioned data sets. We have made a comparison of different S_8 measurements findings which are highlighted in Fig. 4 (right panel) resorting to (*i*) late-time measurements, namely, KiDS-1000 ($S_8 = 0.759^{+0.024}_{-0.021}$) (M. Asgari et al. 2021), KiDS-450 ($S_8 = 0.745^{+0.039}_{-0.039}$) (H. Hildebrandt et al. 2017), DES Y1 ($S_8 = 0.759^{+0.025}_{-0.023}$) (T. M. Abbott et al. 2018), DES Y3 ($S_8 = 0.759^{+0.025}_{-0.023}$) (A. Amon et al. 2022); and (*ii*) early-time measurements, namely Planck 2018 ($S_8 = 0.834^{+0.016}_{-0.016}$) (N. Aghanim et al. 2020), and different values of S_8 is reported from ACT collaboration, the $S_8 = 0.830 \pm 0.043$, 0.840 ± 0.030 and 0.846 ± 0.016, for ACT, ACT + WMAP ACT + WMAP ACT + Planck observations, respectively (more detail is presented in the work S. Aiola et al. 2020).

For instance, the sigma difference between KiDS-1000 and Planck measurements is approximately 2.68σ, indicating a tension. Our results together with the late- and early-time measurements are presented in Fig. 4 (right panel) for all combined data sets. Using the S_8 values from Table 1, the diffusive model differs from Planck measurements by 0.56σ, -0.51σ, and -1.39σ, and differs from

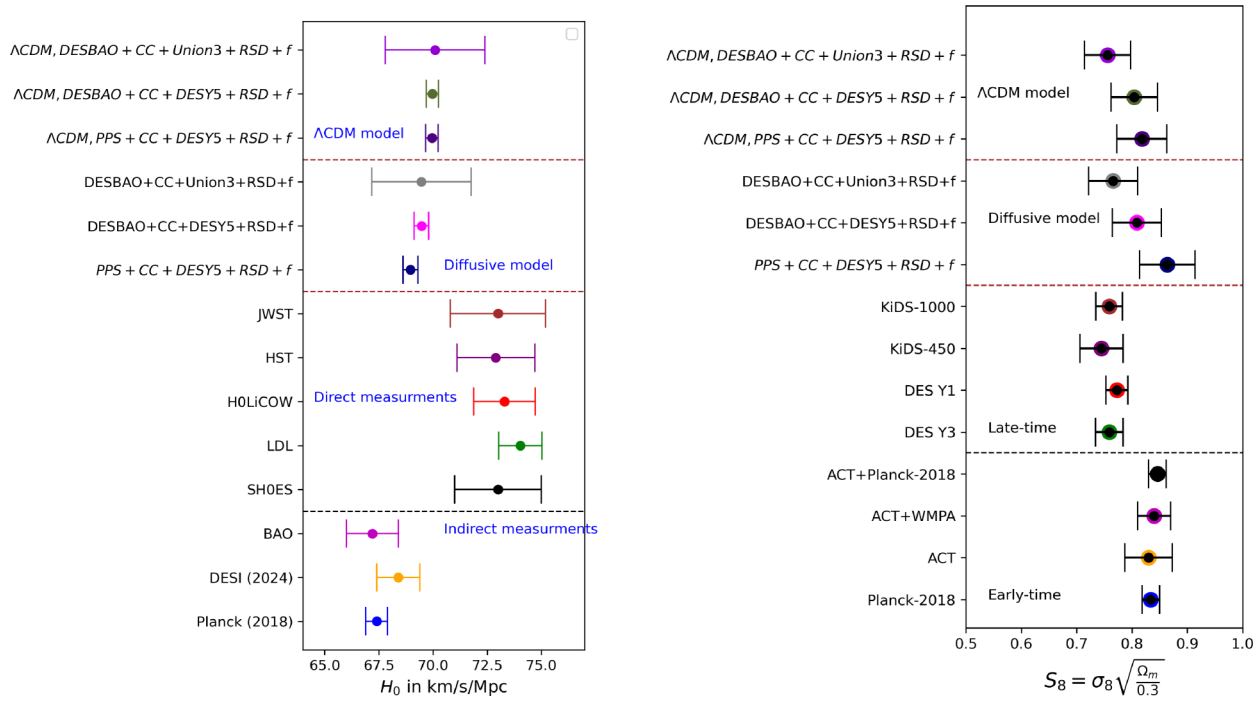

Figure 4. The comparison of ΛCDM and diffusive model H_0 values (in km s^{-1} Mpc^{-1}) with early and direct measurements (left panel), S_8 values between the ΛCDM and diffusive models alongside various late-time and early-time measurements (right panel).

KiDS-1000 by 0.56σ, -0.51σ, and -1.39σ for the *PPS + CC + DESY5 + RSD + f*, *DESI DR2 BAO + CC + DESY5 + RSD + f*, and *DESI DR2 BAO + CC + Union3 + RSD + f* data sets, respectively. In the same way, the ΛCDM model differs from Planck measurements by -0.33σ, -0.65σ, and -1.70σ, and differs from KiDS-1000 by 1.07σ, 0.94σ, and -0.06σ. From this comparison we can conclude that the diffusive model's values of S_8 possibly form a bridge between late- and early-time measurements and has a slightly alleviating the tensions, prompting further investigation to address S_8 tensions. However, addressing both cosmological tensions H_0andS_8 more quantitatively by including the Planck 2018 data is beyond the scope of this study.

3.2 Background evolutions

The Hubble parameter, the deceleration parameter $q(z)$, the effective EoS parameter $w_{\rm eff}(z)$, and the distance modulus $\mu(z)$, from equations (15), (16), (17), and (18), respectively, have also been presented numerically in Fig. 5 to demonstrate the background evolution of the Universe in the diffusive model. As mentioned earlier, we have considered the values of $Q_{\rm dm} = -0.017, -0.013, -0.009$ together with the values of $H_0 = 68.959$, $\Omega_{\rm m} = 0.361$ for the diffusive model and the corresponding values of $\Omega_{\rm m} = 0.310$ and $H_0 = 69.950$ for ΛCDM model taken from Table 1. By emphasizing these key cosmological parameters (i.e. $q(z)$, $w_{\rm eff}(z)$, $H(z)$, $\mu(z)$), we present the numerical results in Fig. 5 to show the implications of the diffusive dark-fluid model in comparison with the ΛCDM model. The deceleration parameter $q(z)$, represented by the upper left of Fig. 5, shows how both models depart from a decelerating Universe to an accelerating Universe at comparable redshifts.

Similarly, in the upper right panel of Fig. 5, the effective EoS $w_{\rm eff}(z)$ demonstrates a key difference between the two models. This dynamic behaviour could offer a more accurate explanation for the accelerated expansion observed today and potentially alter predictions about the cosmic expansion. In the bottom left of Fig. 5, the Hubble parameter $H(z)$ of both models with the observational data is presented. Finally, the bottom right panel of Fig. 5, which shows the distance–redshift relation $\mu(z)$, compares predictions for the distance–redshift relation using Pantheon+SH0ES data. Both models are consistent with the supernova data, but minor deviations between the models at higher redshifts may hint at the diffusive dark-fluid model offering a different interpretation of the role DE played in the past.

As a result, these plots presented in Fig. 5 show that the cosmic expansion rate is sped up consistently for all cases of $Q_{\rm dm} < 0$. Particularly, in the past cosmic evolution $z > 0$, higher deviations are significantly noticeable, which indicates that the flow of energy is insightful. Conversely, when $Q_{\rm dm} < 0$, energy transfers from DM to DE, leading to an enhancement of cosmic acceleration. Later in Section 3.3, we shall pay attention to how the sign of $Q_{\rm dm}$ changes the phase of the Universe. In the current Universe ($z = 0$), the diffusive dark-fluid model has a minimal deviation from the ΛCDM model, and this deviation is also significantly visible at higher redshifts, exhibiting variations that suggest a distinct rate of acceleration in the early Universe. This implies that the diffusive dark-fluid model might offer new insights into how the acceleration of the Universe's expansion evolved.

3.3 State finder diagnostics

In this section, we consider the parameters for the state finder, r and s, which are introduced by V. Sahni et al. (2003) as

$$r \equiv \frac{\dddot{a}}{aH^3} = q(2q+1) + (1+z)\frac{\mathrm{d}q}{\mathrm{d}z}\,, \quad \text{and} \quad s = \frac{r-1}{3(q-\frac{1}{2})}\,, \tag{40}$$

respectively, for a better distinction between diffusive and ΛCDM models. The numerical results of these state-finder diagnostic plots

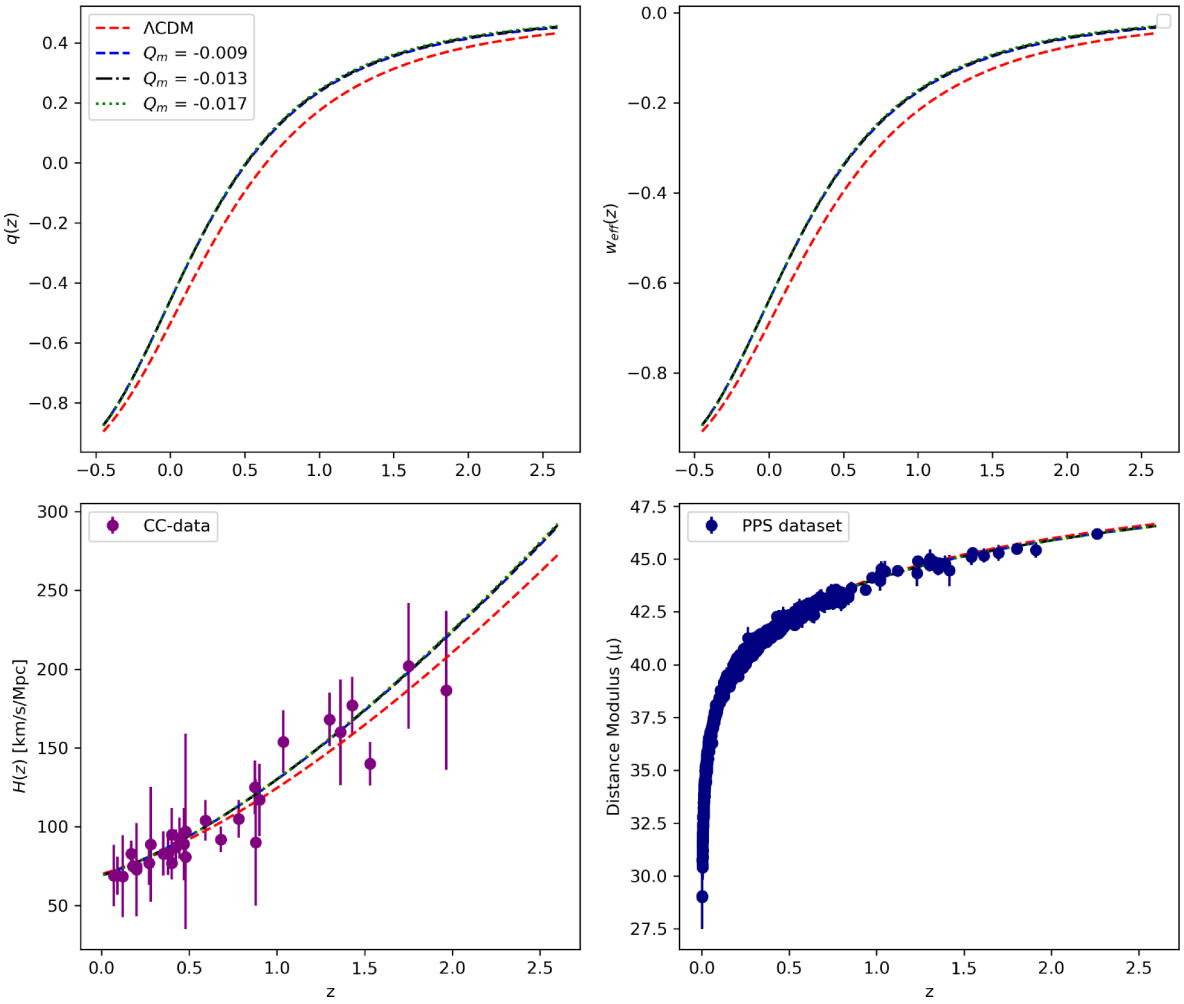

Figure 5. The diagrams for multiple cosmological parameters in both models: diffusive dark-fluid and ΛCDM models are highlighted in this Figure. (i) With slight variations for the diffusive model at higher redshifts, the top-left panel deceleration parameter $q(z)$ depicts the change from deceleration to acceleration. (ii) The effective EoS parameter $w_{\rm eff}(z)$ in both models is shown in the upper-right panel. (iii) The bottom-left panel shows that the CC data for both models fit the Hubble parameter $H(z)$. (iv) The bottom-right panel shows the distance modulus $\mu(z)$, which both models closely match the data with PPS. For illustrative purpose, we use $Q_{\rm dm} = -0.017, -0.013, -0.009$, $H_0 = 68.959$ in km s^{-1} Mpc^{-1}, $\Omega_{\rm m} = 0.361$ for diffusive model and $\Omega_{\rm m} = 0.310$ and $H_0 = 69.950$ in km s^{-1} Mpc^{-1} for ΛCDM model from joint analysis of $PPS + CC + DESY5 + RSD + f$ presented in Table 1.

are shown in Fig. 6. The plot shows the diagram of q versus r (upper panel) and s versus r (bottom panel) for different the values of $Q_{\rm dm}$, offer valuable insights into the nature of cosmic expansion and the role of the diffusive dark-fluid model in comparison to the standard ΛCDM model. Based on the values of the pair r, s, the diffusive dark-fluid model is categorized into the following three classes: for the case of $r > 1$, $s < 0$ where the diffusive model serve as CG model when $Q_{\rm dm} < 0$, for the case of $r < 1$, $s > 0$, where the diffusive model serve as quintessence model when $Q_{\rm dm} > 0$ and $r = 1, s = 0$, the diffusive model serve as ΛCDM when $Q_{\rm dm} = 0$.

These diagnostics help to distinguish between various DE models and understand their impact on the Universe's evolution. In the q versus r plot, the black dot refers to the ΛCDM model, representing a Universe with a cosmological constant driving its accelerated expansion. For all cases of negative value of $Q_{\rm dm}$ behaves like the CG model U. Alam et al. (2003), which implies a late dominance of DE, causing an accelerating expansion. Here, the Universe expands at a faster rate than ΛCDM model, with r-values exceeding 1. Similarly, the s versus r plot (bottom panel) shows that the CG-like model produces faster cosmic expansion, as evidenced by the negative s-values.

We also consider the $Om(z)$ diagnostics which expressed as V. Sahni et al. (2003, 2008)

$$Om(z) = \frac{\left[\frac{H(z)}{H_0}\right]^2 - 1}{(1+z)^3 - 1}\,. \tag{41}$$

We present the numerical results of $Om(z)$ for diffusive models as presented in Fig. 7. From our results, we have noticed that the diffusive model is similar to ΛCDM model, where DE behaves as a cosmological constant (where $Q_{\rm dm} = 0$), $Om(z)$ remains approximately constant at different redshifts. For the case of $Q_{\rm dm} < 0$, $Om(z)$ decreases with cosmic time, and the diffusive model behaves as CG, which leads the cosmic acceleration.

3.4 Structure growth

As mentioned earlier, the coupled equation of the density contrast presented in equations (33) and (34) are taken into account to present

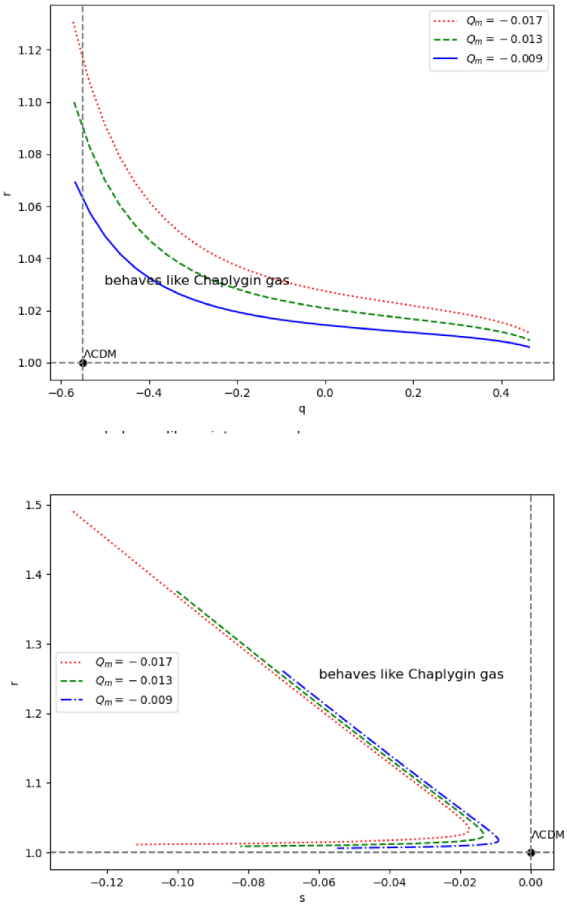

Figure 6. The state finder diagnostic q versus r (left panel) and s versus r (right panel). We use $Q_{\rm dm} = -0.017, -0.013, -0.009$, $H_0 = 68.959$ in km s^{-1} Mpc^{-1}, $\Omega_{\rm m} = 0.361$ for diffusive model and $\Omega_{\rm m} = 0.310$ and $H_0 = 69.950$ in km s^{-1} Mpc^{-1} for ΛCDM model.

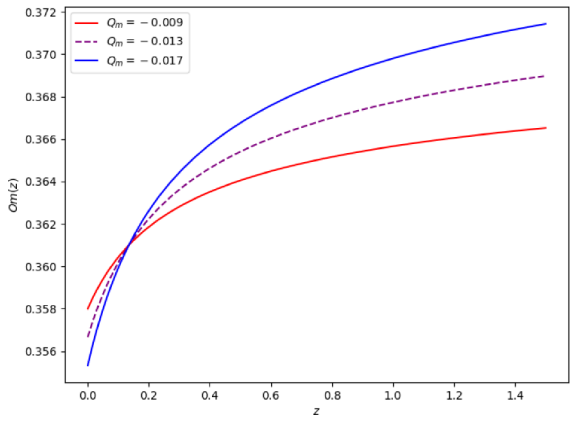

Figure 7. $Om(z)$ diagnostic diagram for the diffusive model for the case of $Q_{\rm dm} = -0.017, -0.013, -0.009$ and $\Omega_{\rm m} = 0.361$.

the numerical results of $\delta(z)$ for matter and DE using the best-fitting values of $\Omega_{\rm m} = 0.361$ and $Q_{\rm dm} = -0.017, -0.013, -0.009$ taken from Table 1 as shown in Fig. 9. The value of $\delta_{\rm de}(z)$ is generally small compared with the corresponding values of $\delta_{\rm m}(z)$. The figure clearly shows $\delta_{\rm m}(z) >> \delta_{\rm de}(z)$, highlighting the dominant role of matter perturbations in having a significant effect on gravitational collapse, which is the cause of structure formation. Hereafter, we choose the

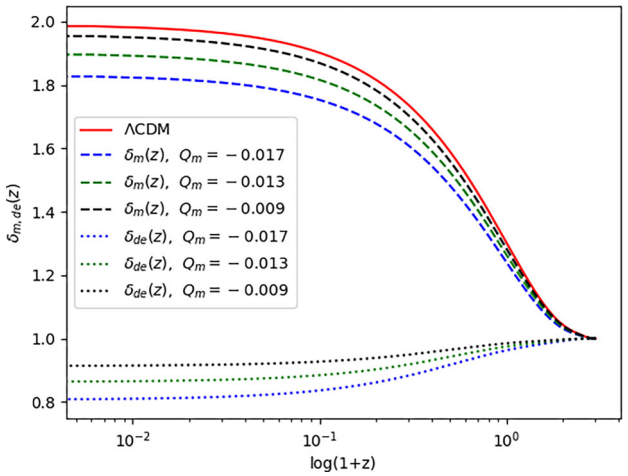

Figure 8. The numerical results of the density contrast $\delta_{de,m}(z)$ (using the coupled system equations 33 and 34) for diffusive cosmology with ΛCDM models. We use $\Omega_m = 0.361$, $Q_{dm} = -0.017, -0.013, -0.009$ and $\Omega_{de} = 1 - \Omega_m$.

density contrast $\delta_{\rm m}(z)$ for further discussion of the growth rate $f(z)$ and the redshift space distortion $f\sigma_8(z)$. In this Figure, the density contrast, $\delta_{\rm m}(z) \geq 1$, indicates that the density contrast grows and becomes more pronounced, leading to non-linear behaviour. In this regime, matter clusters into dense regions, forming structures such as galaxies and galaxy clusters. The plot shows the evolution of the matter density contrast, $\delta_{\rm m}(z)$ as a function of redshift, comparing the standard ΛCDM model (solid red curve) with the diffusive dark-fluid model characterized by different values of $Q_{\rm dm}$ (blue, green, and black dashed curve). In the diffusive dark-fluid model, with parameters $\Omega_{\rm m} = 0.361$, and $Q_{\rm dm} = -0.017, -0.013, -0.009$, there is a deviation from the ΛCDM model ($\Omega_{\rm m} = 0.310$), showing significant impact enhanced structure formation. Specifically, the model with a negative $Q_{\rm dm} = -0.017$ (blue dashed curve) shows a significant slowing in the structure formation across all redshifts, suggesting that the growth of density fluctuations is more delayed compared to the ΛCDM model. This demonstrates that the diffusion of matter into DE slows gravitational collapse or speeds up the accelerating cosmic expansion, resulting in a slower rate of structure growth.

Additionally, by accounting for the growth rate function presented in equation (37), we present the numerical results of $f(z)$ shown in Fig. 9 (upper panel) for diffusive and ΛCDM models using $Q_{\rm dm} = -0.017, -0.013, -0.009$. In the same manner, the RSD $f\sigma_8$ from equation (39) the diagram of the $f\sigma_8(z)$ has been presented as illustrated in Fig. 9 (bottom panel). These plots compare the diffusive dark-fluid model with the same values of $Q_{\rm dm}$ along with ΛCDM in terms of the growth rate and the redshift space distortion $f\sigma_8$ diagrams. Notably, the diffusive model deviates slightly from the ΛCDM at lower redshifts and exhibits a more pronounced deviation at higher redshifts. This suggests that the impact of energy diffusion between DM and DE has an impact on the growth of structures.

3.5 Statistical analysis

The Bayesian/Schwarz Information Criterion (BIC) and Akaike Information Criterion (AIC) are used in our statistical analysis to evaluate the suitability of diffusive models compared to ΛCDM. As broadly described in the work (A. R. Liddle 2009; M. Szydłowski

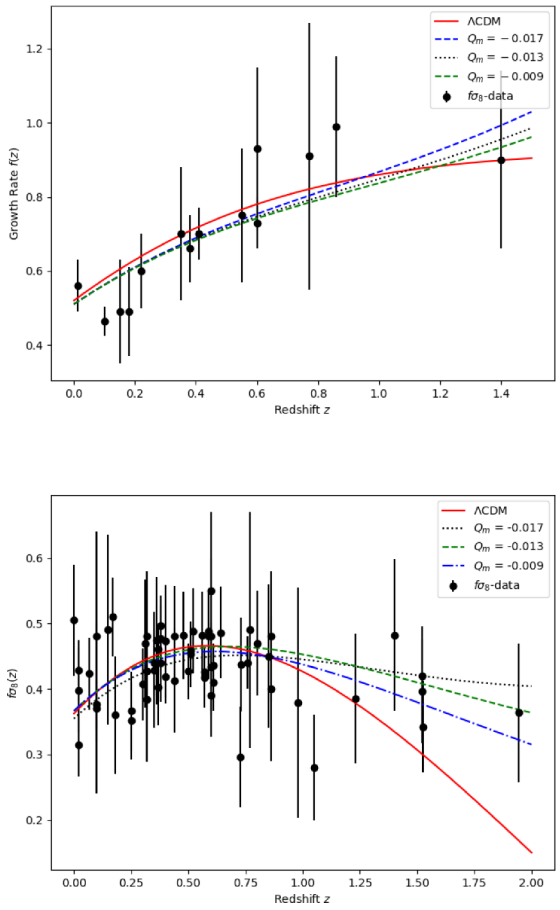

Figure 9. Upper panel: the numerical results of the growth rate $f(z)$ from equation (37) for both theories: ΛCDM and diffusive dark-fluid models with observational growth rate data with error bars. Bottom panel: the diagram of the $f\sigma_8(z)$ from using equation (39) as a function of redshift z using $Q_{\rm dm} = -0.017, -0.013, -0.009$. The observational data points are shown with error bars.

et al. 2015; M. Rezaei & M. Malekjani 2021), we consider the statistical computations BIC and AIC to determine if the diffusive model should be 'accepted' or 'rejected' in comparison to ΛCDM. We use the ΛCDM as the 'accepted' model for comparison to support our claims using the AIC and BIC criteria. By using these standards, we can determine if the diffusive model will be accepted or rejected. The following relations are used for calculating the AIC and BIC values in the ΛCDM and diffusive models: $\mathrm{AIC} = \chi^2 + 2\mathrm{K}$, and $\mathrm{BIC} = \chi^2 + \mathrm{K}\log(\mathrm{N_i})$, where χ^2 is computed using the model's Gaussian likelihood function $\mathcal{L}(\hat{\Theta}|\mathrm{data})$, the number of free parameters for that specific model is K. At the same time, N_i is the number of data points for the i^{th} data set. Consequently, by defining the AIC Bayes factor,

$$\Delta\mathrm{AIC} = \left|\mathrm{AIC}_{\rm Diffusive} - \mathrm{AIC}_{\Lambda\rm CDM}\right| ,$$

where $\Delta\mathrm{AIC} \leq 2$ indicates that the proposed theoretical model holds a substantial observational support for the fitted data, $4 \leq \Delta\mathrm{AIC} \leq 7$ indicates less observational support, and finally $\Delta\mathrm{AIC} \geq 10$ indicates no observational support as stated in (M. Szydłowski et al. 2015). The BIC Bayes factor can also be expressed as follows:

$$\Delta\mathrm{BIC} \equiv 2\ln\mathrm{BIC} = -(\mathrm{BIC}_i - \mathrm{BIC}_j) ,$$

where $2\ln\mathrm{BIC}$ is the BIC Bayes factor comparing model (i) against model (j). In this case, (i) stands for the ΛCDM model, and (j) for the diffusive model. The following is a ranking of the evidence against ΛCDM, i.e. in favour of the diffusive model, based on the categorization in M. Szydłowski et al. (2015) is negligible if $0 \leq 2\ln\mathrm{BIC} \leq 2$, positive if $2 \leq \Delta\mathrm{BIC} \leq 6$, strong if $6 \leq \Delta\mathrm{BIC} \leq 10$, and extremely strong if $\Delta\mathrm{BIC} > 10$, see Table 2 for more details. Table 2 displays the complete model's comparison, and the findings indicate that all values of ΔAIC are less than 2. According to ΔAIC, this implies that the diffusive model is competitive with ΛCDM. However, the values of ΔBIC fall within the range of $2 \leq \Delta\mathrm{BIC} \leq 6.080$. This suggests that there is strong evidence against ΛCDM in favour of the diffusive model. Based on the work in D. Parkinson et al. (2005) and M. Biesiada (2007), due to the large number of data N_i such as PPS and DESY5, AIC tends to favour models with more parameters. In contrast, BIC tends to penalize them. Even the recent work S. Sahlu et al. (2025b) highlighted a similar approach, regarding the model is more penalized by BIC because of the more data points. However, the statistical preference remains moderate, meaning that while the diffusive model demonstrates potential advantages or consistency with certain observations, the level of support is not yet compelling enough to favour it decisively over ΛCDM. More observational data, theoretical refinements, and robustness checks are necessary to determine whether the diffusive model can provide an explanation of cosmic dynamics compared to the ΛCDM framework.

4 CONCLUSION

In the current manuscript, the implications of the diffusive model for late-time cosmology and the evolution of cosmic structures in which DM and DE interact via energy exchange have been investigated. In this paradigm, we assume that the sign of the interaction component, $Q_{\rm dm}$, determines the direction of energy transfer between DM and DE. A negative interaction term $-Q_{\rm dm}$ implies the transfer of energy from DM to DE, allowing the diffusive component to serve as an effective DE. This energy transfer causes cosmic acceleration while limiting the growth of structures, whereas a positive interaction term has the reverse effect.

To provide a comprehensive understanding, the background evolution and perturbation equations within the diffusive model have been derived, and the best-fitting values of cosmological parameters are obtained through MCMC simulations, with the results summarized in Table 1. In parameter constraints analysis, the values of H_0 in $\mathrm{km\,s^{-1}\,Mpc^{-1}}$, $\Omega_{\rm m}$, $r_{\rm d}$, M, σ_8, S_8 and the interaction term $Q_{\rm dm}$. From the constrained best-fitting values (see Table 1), we notice that the interaction term has a negative sign across all observational data. The background evolution results given, particularly the diagnostic diagram of the state finder, show that the diffusive model behaves like a CG. This suggests that the diffusive dark-fluid cosmology is a promising model as an alternative to DE, serving as the driving force for late-time cosmic acceleration through the exchange of energy via a diffusive mechanism from the DM component to DE. This investigation is also supported by the work presented in S. Calogero & H. Velten (2013). By considering the 95 per cent of C.L of the values of the interacting term $Q_{\rm dm} = -0.013^{+0.004}_{-0.004} = -0.017, -0.013, -0.009$ taken from Table 1 using $PPS + CC + DESY5 + RSD + f$ data sets, the numerical results of $q(z)$, $w_{\rm eff}(z)$, $H(z)$, $\mu(z)$, the state finder parameters (r versus q and r versus s) the diagnostic of $Om(z)$ are presented (see Figs 5–7) to understand the late time cosmology. The investigated parameters, such as r, q, and s, let cosmologists quantify the deviations of the diffusive dark-fluid model from the conventional ΛCDM model. Using these state-finder diagnostics, a powerful tool in cosmology that allows

Table 2. Comparison of statistical estimators $\mathcal{L}(\hat{\Theta}|\text{data})$, χ^2, reduced χ^2_ν, AIC, ΔAIC, BIC, and ΔBIC between the ΛCDM and diffusive dark-fluid models for various data set combinations.

Data combination	**Model**	$\mathcal{L}(\hat{\Theta}\|\text{data})$	χ^2	χ^2_ν	AIC	ΔAIC	BIC	ΔBIC
DESI DR2 BAO + *CC* +	Diffusive	−66.630	131.26	0.924	143.265	1.322	158.212	5.690
Union3 + *RSD* + f	ΛCDM	−66.971	133.942	0.936	141.942	–	153.903	–
DESI DR2 BAO + *CC* + *DESY5*	Diffusive	−919.250	1838.5	1.049	1848.500	0.410	1875.927	5.120
+ *Union3* + *RSD* + f	ΛCDM	−920.456	1840.912	1.049	1848.912	–	1870.799	–
PPS + *CC* + *DESY5* +	Diffusive	−1698.103	3396.206	0.987	3407.206	1.060	3436.930	6.080
RSD + f	ΛCDM	−1699.133	3398.266	0.987	3408.266	–	3430.845	–

us to classify and differentiate between various DE models based on their expansion histories. In our case, the diffusive model with a negative $Q_{\rm dm}$ highlights for the Universe's expansion behaving like the CG model, which has implications for the nature of DE. From the result, we noticed that the diffusive model proves more accurate than the ΛCDM model, which could suggest that DE evolves rather than remains constant.

We also extended the work to investigate further the scalar perturbations leading to structure formation. We demonstrated the growth of matter density contrast $\delta(z)$ and redshift space distortion $f\sigma_8(z)$ through redshift for the interaction term $Q_{\rm dm} = -0.017, -0.013, -0.009$. The results presented in Fig. 9 take into account the coupled system of equations (33) and (34), showing that non-vanishing the non-vanishing cosmological perturbation of DE. However, the result is strongly favoured for the $\delta_{\rm m}(z) \gg \delta_{\rm de}(z)$, which leads to the DM component making a significant contribution to structure formation. We also noticed that from the results of Fig. 9, a slower rate of structure growth for the case of a higher negative values interacting term $Q_{\rm dm} = -0.017$ compared with $Q_{\rm dm} = -0.009$. We also present the diagram of the redshift space distortion $f\sigma_8(z)$ as presented in Fig. 9, and the plot shows that the diffusive model has a minor deviation from the ΛCDM at the lower redshift for all values of the interaction term. However, at a higher redshift, the two models have a higher deviation, which suggests the impact of energy diffusion between DM and DE on the growth of structures at an early stage. Then a detailed statistical analysis was calculated, which includes $\mathcal{L}(\hat{\Theta}|\text{data})$, χ^2, χ^2_ν, AIC, ΔAIC, BIC, and ΔBIC (see Table 2). For all data sets, the $\Delta\text{AIC} \leq 1.322$ showed strong support for the suggested diffusive model, whereas based on the ΔBIC criteria, $\Delta\text{BIC} \leq 6.080$, indicated a considerable positive support against the ΛCDM model.

The current work is an exploration of the viability of the diffusive cosmological model; it needs to be tested against more existing and upcoming data before any conclusive support for or against it is pronounced. One such data left for future work, for example, is that of the CMB, as testing the diffusive model against such data will also give us quantitative clues regarding its ability to reduce the cosmological tensions.

ACKNOWLEDGEMENTS

AA acknowledges that this work is based on research supported in part by the National Research Foundation (NRF) of South Africa (grant no. 112131). This work was part of the research programme "New Insights into Astrophysics and Cosmology with Theoretical Models Confronting Observational Data" of the National Institute for Theoretical and Computational Sciences of South Africa.

DATA AVAILABILITY

We have used the publicly available cosmological probes, as listed in Section 3.

REFERENCES

Abbott T. M. et al., 2018, Phys. Rev. D, 98, 043526
Abdul-Karim M. et al., 2025, Phys. Rev. D, 112, 083515
Abebe A. et al., 2012b, Class. Quantum Gravity, 29, 135011
Abebe A. et al., 2012a, Classical and quantum gravity, 29, 135011
Abebe A. et al., 2013, Phys. Rev. D, 88, 044050
Adame A. et al., 2025, J. Cosmol. Astropart. Phys., 2025, 021
Afroz S., Mukherjee S., 2025, preprint (arXiv:2504.16868)
Aghanim N. et al., 2020, A&A, 641, A6
Aiola S. et al., 2020, J. Cosmol. Astropart. Phys., 2020, 047
Alam U. et al., 2003, MNRAS, 344, 1057
Amon A. et al., 2022, Phys. Rev. D, 105, 023514
Andrade U. et al., 2025, Phys. Rev. D, 112, 083512
Arbey A., 2006, Phys. Rev. D, 74, 043516
Asgari M. et al., 2021, A&A, 645, A104
Bahamonde S. et al., 2017, Phys. Lett. B, 766, 225
Bamba K. et al., 2012, Ap&SS, 342, 155
Bardeen J. M., 1980, Phys. Rev. D, 22, 1882
Benisty D. et al., 2019, Phys. Rev. D, 99, 123521
Bento M. C. et al., 2002a, Phys. Rev. D, 66, 043507
Bento M. C. et al., 2002b, Phys. Rev. D, 66, 043507
Bento M. C. et al., 2004, Phys. Rev. D, 70, 083519
Bento M. d. C. et al., 2003, Phys. Rev. D, 67, 063003
Bergström L., 2009, New J. Phys., 11, 105006
Biesiada M., 2007, J. Cosmol. Astropart. Phys., 2007, 003
Bolejko K. et al., 2011, Class. Quantum Gravity, 28, 164002
Bolotin Y. L. et al., 2015, Int. J. Mod. Phys. D, 24, 1530007
Brout D. et al., 2022, ApJ, 938, 110
Bruni M., et al., 1992, Class. Quantum Gravity, 9, 921
Calogero S., 2011, J. Cosmol. Astropart. Phys., 2011, 016
Calogero S., 2012, J. Geom. Phys., 62, 2208
Calogero S., Velten H., 2013, J. Cosmol. Astropart. Phys., 2013, 025
Cardone V. F. et al., 2012, Phys. Rev. D, 85, 124007
Carloni S. et al., 2008, Phys. Rev. D, 77, 024024
Carroll S. M., 2001, Living Rev. Relativ., 4, 1
Chakraborty A., Chanda P. K., Das S., Dutta K., 2025, JCAP, 11, 047
Colafrancesco S., Profumo S., Ullio P., 2006, A&A, 455, 21
Chiba R., Moriya T. J., 2024, ApJ, 973, 14
Csaki C. et al., 2006, J. Cosmol. Astropart. Phys., 2006, 022
Di Valentino E., 2021, MNRAS, 502, 2065
Di Valentino E. et al., 2021a, Astropart. Phys., 131, 102604
Di Valentino E. et al., 2021c, Astropart. Phys., 131, 102605
Dunsby P., Bruni M., Ellis G., 1992, ApJ, 395, 34
Dunsby P. K. et al., 1992, ApJ, 395, 54
Elizalde E. et al., 2004, Phys. Rev. D, 70, 043539
Ellis G., Bruni M., Hwang J., 1990, Phys. Rev. D, 42, 1035
Ellis G. F., Bruni M., 1989a, Phys. Rev. D, 40, 1804
Ellis G. F., Bruni M., 1989b, Phys. Rev. D, 40, 1804

Fabris J., Goncalves S., De Souza P., 2002, Gen. Relativ. Gravit., 34, 2111
Foreman-Mackey D. et al., 2013, PASP, 125, 306
Gidelew A. A., 2009, Msc thesis, Univ. Cape Town
Haba Z., 2010, Mod. Phys. Lett. A, 25, 2683
Haba Z., Stachowski A., Szydłowski M., 2016, J. Cosmol. Astropart. Phys., 2016, 024
Hamilton A., 1998, The Evolving Universe: Selected Topics on Large-Scale Structure and on the Properties of Galaxies. Kluwer, Dordrecht, p. 185
Hawking S. W., 1966, ApJ, 145, 544
He J.-H., Wang B., Jing Y., 2009, J. Cosmol. Astropart. Phys., 2009, 030
Hildebrandt H. et al., 2017, MNRAS, 465, 1454
Hough R., et al., 2020, Eur. Phys. J. C, 80, 787
Kazantzidis L., Perivolaropoulos L., 2018, Phys. Rev. D, 97, 103503
Kodama H., Sasaki M., 1984, Prog. Theor. Phys. Suppl., 78, 1
Krasinski A., 1997, Inhomogeneous Cosmological Models. Cambridge Univ. Press, Cambridge
Labbe I., et al., 2023, Nature, 616, 266
Lewis A., 2019, preprint (arXiv:1910.13970)
Liddle A. R., 2009, Annu. Rev. Nucl. Part. Sci., 59, 95
Lifshitz E. M., 1946, J. Phys., 10, 116
Louis P. et al., 2019, J. Cosmol. Astropart. Phys., 6, 20
Maity S. et al., 2019, Eur. Phys. J. C, 79, 1
Mekuria R. R., 2017, PhD thesis, Univ. Witwatersrand
Mekuria R. R., 2019, Proc. IAU Symp. 15, Nuclear Activity in Galaxies Across Cosmic Time. p. 390
Mekuria R. R., Colafrancesco S., Faltenbacher A., Marchegiani P., 2017, Proc. Sci., HEASA 2016. SISSA, Trieste, PoS#009
Milgrom M., 1983, ApJ, 270, 365
Moresco M. et al., 2020, ApJ, 898, 82
Mukhopadhyay U. et al., 2020, Eur. Phys. J. C, 80, 904
Mukhopadhyay U. et al., 2021, Phys. Rev. D, 103, 063510
Myrzakulov R., 2011, Eur. Phys. J. C, 71, 1752
Naidoo K. et al., 2024, Phys. Rev. D, 109, 083511
Ntahompagaze J. et al., 2018, Int. J. Mod. Phys. D, 27, 1850033
Ntahompagaze J. et al., 2020, Int. J. Mod. Phys. D, 29, 2050120
Nunes R. C., Vagnozzi S., 2021, MNRAS, 505, 5427
Nunes R. C. et al., 2016, Phys. Rev. D, 94, 023508
Olson D., 1976, Phys. Rev. D, 14, 327
Parkinson D. et al., 2005, Phys. Rev. D, 71, 063524
Peebles P., Ratra B., 1988, ApJ, 325, L17
Peebles P. J., 1999, Nature, 398, 25
Qi J.-Z. et al., 2023, Phys. Rev. D, 108, 063522
Rezaei M., Malekjani M., 2021, Eur. Phys. J. Plus, 136, 219
Riess A. G. et al., 2011, ApJ, 730, 119
Riess A. G. et al., 2019, ApJ, 876, 85
Riess A. G. et al., 2022, Astrophys. J. Lett., 934, L7
Rubin D. et al., 2025, Astrophys. J., 986, 231
Sahlu S., Ntahompagaze J., Abebe A., Mota D. F., 2021, Proc. IAU Symp. 15, Nuclear Activity in Galaxies Across Cosmic Time. p. 397
Sahlu S. et al., 2019b, Eur. Phys. J. C, 79, 1
Sahlu S. et al., 2020, Eur. Phys. J. C, 80, 422
Sahlu S. et al., 2023, Int. J. Mod. Phys. D, 32, 2350090
Sahlu S. et al., 2024, Eur. Phys. J. C, 84, 982
Sahlu S., Hough R. T., Abebe A., de la Cruz-Dombriz Á., 2025a, Eur. Phys. J. C, 85, 746
Sahlu S., de la Cruz-Dombriz Á., Abebe A., 2025b, MNRAS, 539, 690
Sahni V. et al., 2003, J. Exp. Theor. Phys. Lett., 77, 201
Sahni V. et al., 2008, Phys. Rev. D, 78, 103502
Sami H. et al., 2021, Eur. Phys. J. C, 81, 1
Saridakis E. N. et al., 2021, Modified Gravity and Cosmology. Springer-Verlag, Berlin
Sharov G. S. et al., 2017, MNRAS, 466, 3497
Silva E., Sabogal M. A., Scherer M., Nunes R. C., Di Valentino E., Kumar S., 2025, Phys. Rev. D, 111, 123511
Skara F., Perivolaropoulos L., 2020, Phys. Rev. D, 101, 063521
Solanki R. et al., 2022, Phys. Dark Universe, 36, 101053
Springel V. et al., 2006, Nature, 440, 1137
Szydłowski M. et al., 2015, Eur. Phys. J. C, 75, 5
Velten H. E. et al., 2014, Eur. Phys. J. C, 74, 1
Verde L. et al., 2019, Nat. Astron., 3, 891
Wang B. et al., 2007, Nucl. Phys. B, 778, 69
Wang B. et al., 2016, Rep. Prog. Phys., 79, 096901
Weinberg S., 1989, Rev. Mod. Phys., 61, 1
van der Westhuizen M., Figueruelo D., Thubisi R., Sahlu S., Abebe A., Paliathanasis A., 2025, Phys. Dark Univ., 50, 102107
Van der Westhuizen M. A., Abebe A., 2024, J. Cosmol. Astropart. Phys., 2024, 048
Wong K. C., et al., 2020, MNRAS, 498, 1420
Woodfinden A. et al., 2022, MNRAS, 516, 4307
Yang W., Xu L., 2014, Phys. Rev. D, 89, 083517
Zhai Y., et al., 2023, J. Cosmol. Astropart. Phys., 2023, 032
Zhang T., Li X., 2007, Phys. Lett. B, 663, 382
Zimdahl W., 2005, Int. J. Mod. Phys. D, 14, 2319

This paper has been typeset from a TEX/LATEX file prepared by the author.